

UNIVERSITY OF READING
SCHOOL OF MATHEMATICAL AND PHYSICAL SCIENCES

WAVE REFLECTION AND TRAPPING IN A TWO DIMENSIONAL
DUCT

TAHNIA APPASAWMY

AUGUST 2010

Supervisors:

Dr. Nick BIGGS & Dr. Peter CHAMBERLAIN

This dissertation is submitted to the Department of Mathematics in partial fulfilment of
the requirements for the degree of Master of Science

Abstract

Trapped modes occur in many areas in physics, we will be investigating their existence in an acoustic waveguide using Dirichlet and Neumann boundary conditions. We choose to find these trapped modes through a perturbation method and numerically solve the problem. Further investigations will deal with the geometric structure of the waveguide and discuss the existence of these modes in various situations.

I would like to thank, both my supervisors Nick Biggs and Peter Chamberlain for their time, patience and encouragement throughout this experience. It has been more than appreciated!

Contents

1	Introduction	1
2	Boundary Wave Problem	2
2.1	The Dirichlet Problem	2
2.2	Perturbation method	4
2.3	The Reflective Wave in a Tapered Duct	9
2.4	A Uniform Expansion for a reflecting wave in a tapered duct	13
2.5	Trapping of waves in a symmetric duct	19
3	The Neumann Problem	20
4	The Numerical Approach	23
4.1	Plotting solutions of k	23
4.2	Plotting the final solutions with Dirichlet boundary conditions	28
4.3	Plotting the final solutions with Neumann boundary conditions	33
4.4	Varying the small parameter ϵ	40
4.5	Changing the geometrical structure	42
4.6	The Neumann boundary condition for the waveguide where $h_- = 1$	48
5	Conclusion	50
6	First Appendix	51
7	Bibliography	52

List of Figures

1	The waves propagating in the waveguide.	3
2	Diagram illustrating a tapered duct	9
3	Solutions to wavenumbers of antisymmetric trapped modes for $n=1$ are plotted for each Airy solution, with the first solution Z_1 plotted as the lowest line increasing up to Z_n for $n=24$	24
4	Solution to wavenumbers of symmetric trapped modes for $n=1$ are plotted for each Airy solution with the first solution Z'_1 plotted as the lowest line increasing up to Z_n for $n=24$	25
5	Wavenumbers of antisymmetric trapped modes for $n=2$	26
6	Wavenumbers of symmetric trapped modes for $n=2$	27
7	Contour plot of antisymmetric trapped modes.	28
8	Contour plot of the symmetric trapped modes.	29
9	Surface plot of antisymmetric trapped modes, where we let $h_1 = 1.224$ and wavenumber $k = 1.500052$	30
10	Surface plot of the symmetric trapped modes, where we let $h_1 = 1.224$ and wavenumber $k = 1.479089$	31
11	Contour plot of antisymmetric trapped modes for $n=2$	32
12	Contour plot of symmetric trapped modes for $n=2$	33
13	Contour plot of antisymmetric trapped modes, with Neumann boundary condition.	34
14	Contour plot of the symmetric trapped modes, with Neumann boundary condition for $n = 1$	35
15	Surface plot of antisymmetric trapped modes, with Neumann boundary condition for $n = 1$, where we let $h_1 = 1.224$ and wavenumber $k = 1.500052$. . .	36
16	Surface plot of the symmetric trapped modes, with Neumann boundary condition for $n=1$, where we let $h_1 = 1.224$ and wavenumber $k = 1.479089$. . .	37
17	Contour plot of antisymmetric trapped modes, with Neumann boundary condition for $n=2$	38
18	Contour plot of the symmetric trapped modes, with Neumann boundary condition for $n=2$	39
19	Contour plot of antisymmetric modes, with Neumann condition for $\epsilon = 0.001$	40
20	Contour plot of symmetric modes with Dirichlet condition for $\epsilon = 0.001$. . .	41
21	Waveguide with a bulging upper profile, and constant lower profile	42

22	Contour plot of antisymmetric modes, with Dirichlet condition for the new geometrical structure.	43
23	Contour plot of symmetric modes with Dirichlet condition for the new geometrical structure.	44
24	Surface plot of symmetric modes with Dirichlet condition for the new geometrical structure, where $h = 1.3012$ and $k = 1.54682$	45
25	Contour plot of antisymmetric modes, with Dirichlet condition for the new geometrical structure, when $n = 2$	46
26	Contour plot of symmetric modes with Dirichlet condition for the new geometrical structure, when $n = 2$	47
27	Contour plot of antisymmetric modes with Neumann condition for the new geometrical structure, when $n = 1$	48
28	Contour plot of symmetric modes with Neumann condition for the new geometrical structure, when $n = 1$	49

1 Introduction

Trapped modes are related to the eigenvalues of a homogeneous differential equation. It is physically represented by free oscillations of finite energy within a localised slowly varying region. These oscillations occur at very precise frequencies and as a result of their geometrical structure have a cut-off frequency which exponentially decays along the straight waveguide. [2, 5]

Applications in this area are numerous and varies in a range of fields. For example, re-searching trapped modes in water waveguides, to electromagnetic, quantum and acoustic waveguides. In particular, evidence from a paper by Parker and Stoneman (1989) [6] suggest that the vortex shedding, which is an unsteady flow generated by low pressure zones caused by waves at a critical velocity flowing past a blunt object. When the vortex shedding frequency is near an acoustic resonance frequency the two frequencies match, resulting in a resonant frequency and so by the acoustic resonance in this case may control the shedding process. By considering high amplitude oscillations we can control the vortex shedding or change the geometry of the resonator.

Another application this work may be useful to are instrument builders particularly flute makers, as they must take into consideration the length, thickness and specific curvature of the flute tube to construct the standard pitching for the concert flute and the ranges in the flute family.

Investigating trapped modes in general suggest a build up of energy, resulting in resonance, an important phenomenon in physics. By identifying these modes in the fields already mentioned, experts are able to apply or dampen the effect to their advantage. In this paper we will be dealing with finding trapped modes numerically in an acoustic waveguide.

The existence of trapped modes depend on a range of factors. In particular the structural curvature of the waveguide relative to the surface boundary condition. [3]. In other words, certain boundary conditions for specifically shaped waveguides, produce trappings. The symmetry of the waveguide also has an effect. In this paper, we will be considering a symmetric waveguide, to simplify the problem. As it has been proven that existence of antisymmetric modes occur about the centreline of the guide, yet disappear for wavenumbers below the cut-off frequency. [2, 3]. However experimental studies have been made in antisymmetric waveguides, but again, existence in trappings also depend on the geometric structure of the guide. The group velocity of the wave is the velocity of the waves amplitude, and this also has an effect, for example, some modes propagate with a thin region but cut-off by a thicker region in the guide with a negative group velocity.[2].

This paper will deal with a slowly varying waveguide with the geometry of symmetrically

tapered duct. We will investigate the existence of the modes, with two different boundary conditions. This paper will investigate and compare trappings with Dirichlet and Neumann boundary conditions.

Having considered the duct walls to be slowly varying, such that it varies on a length scale inversely proportional to some parameter $0 < \epsilon \ll 1$, which produces a smoother function for the boundary. The problem itself, is solved by the Helmholtz equation. We can analytically solve the problem by a perturbation method, similar to the WKBJ (Wentzel, Kramers, Brioullin, Jeffreys) Method. This approximation method transforms a wavefunction into an exponential function, and approximates the solution of the differential equation, with a small parameter ϵ , say, in the highest derivative term.

[7] This paper will also look at the numerical calculations of the modes and a general solution to the problem, applying a similar approach used by Postnova and Craser. We will compare the results of the different boundary conditions and discuss further advances to be made to this paper.

2 Boundary Wave Problem

2.1 The Dirichlet Problem

Consider a two-dimensional acoustic waveguide, with the motion of the waves entering duct with an infinite range in the x -direction, tapered at on each end. The function ϕ will be in terms of the Cartesian coordinates, given in 2-dimensional space. The wavefield $\phi(x, y)$ satisfies the Helmholtz equation

$$\bar{\phi}_{\bar{x}\bar{x}} + \bar{\phi}_{\bar{y}\bar{y}} + \bar{k}^2 \bar{\phi} = 0 \quad (-\infty < \bar{x} < \infty, -\bar{h}_-(\bar{x}) < \bar{y} < \bar{h}_+(\bar{x})), \quad (1)$$

Here k is the wavenumber and $y = \pm \bar{h}_{\pm}(\bar{x})$ are the upper and lower boundaries of the waveguide respectively.

We may now consider the boundary conditions of our problem. These are

$$\bar{\phi} = 0 \quad (-\infty < \bar{x} < \infty, \bar{y} = \pm \bar{h}_{\pm}(\bar{x})), \quad (2)$$

$$\bar{\phi} \rightarrow 0 \quad \text{as } \bar{x} \rightarrow \pm\infty. \quad (3)$$

Equation (2) is the Dirichlet boundary condition of our problem. We now solve the problem using an asymptotic approach.

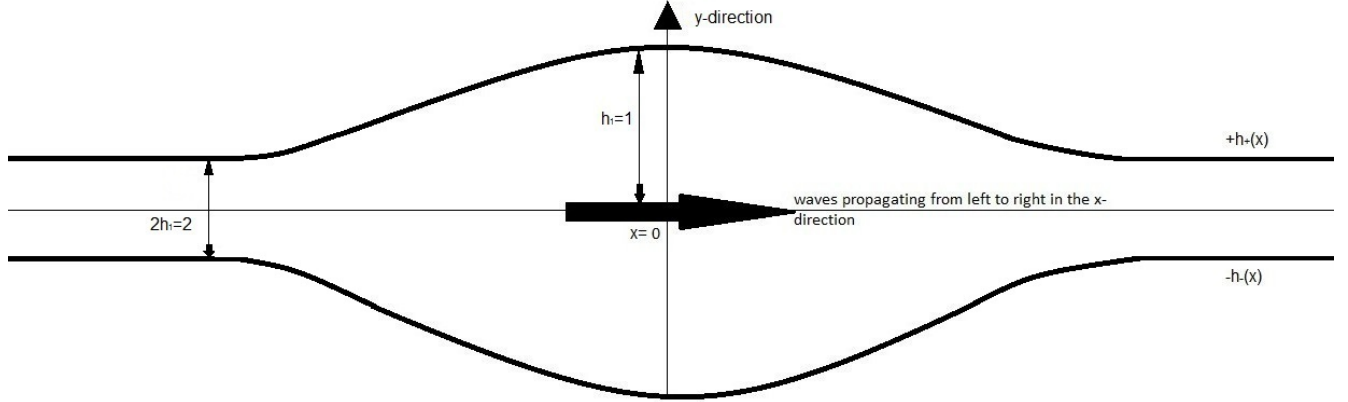


Figure 1: The waves propagating in the waveguide.

Our first step is to non-dimensionalise the variables using the scaled equations below

$$x = \epsilon \bar{x} / h_0, \quad (4)$$

$$y = \bar{y} / h_0, \quad (5)$$

$$k = \bar{k} h_0, \quad (6)$$

$$\phi(x, y) = \bar{\phi}(\bar{x}, \bar{y}), \quad (7)$$

and

$$h_{\pm}(x) = \frac{\bar{h}_{\pm}(\bar{x})}{h_0}, \quad (8)$$

for some positive h_0 , and $h_{\pm}(x)$ are the non-dimensionalised functions calculating the structure of the waveguide, the function is determined by,

$$h_{\pm}(x) = 1 + (h_1 - 1) \operatorname{sech}(x). \quad (9)$$

Figure (1) illustrates the slowly varying waveguide, where h_1 is the length from the top of the bulge to the x -axis, a positive constant we let $= 1$. The ϵ term in equation (4) is a small variable, relating to the slowly varying guide.

If we now substitute the non-dimensional equations into equation (1), we see that the terms

non dimensionalise in the following way:

$$\bar{\phi}_{\bar{x}} = \phi_x x_{\bar{x}} = \frac{\epsilon}{h_0} \phi_x \quad \text{thus } \bar{\phi}_{\bar{x}\bar{x}} = \left(\frac{\epsilon}{h_0}\right)^2 \phi_{xx} \quad (10)$$

Similarly the second term non-dimensionalises as

$$\bar{\phi}_{\bar{y}\bar{y}} = \frac{\phi_{yy}}{h_0^2} \quad (11)$$

This leads to the assembled equation

$$\left(\frac{\epsilon}{h_0}\right)^2 \phi_{xx} + \frac{\phi_{yy}}{h_0^2} + \left(\frac{k}{h_0}\right)^2 \phi = 0 \quad (12)$$

This then simplifies to

$$\epsilon^2 \phi_{xx} + \phi_{yy} + k^2 \phi = 0, \quad (13)$$

together with the non-dimensionalised boundary conditions

$$\phi = 0 \quad (-\infty < x < \infty, y = \pm h_{\pm}(x)), \quad (14)$$

$$\phi \rightarrow 0 \quad \text{as } x \rightarrow \pm\infty. \quad (15)$$

2.2 Perturbation method

We are now able to construct an asymptotic expansion in powers of the small parameter ϵ using a perturbation method closely related to the WKBJ theory. The method is an approximation to the characteristics of the waves in a slowly varying waveguide. The wave function $\phi(x, y)$ can be written as an exponential of another function ϕ , such that

$$\phi = A(x, y)e^{P(x, y)}, \quad (16)$$

where

$$A = A_0(x, y) + \epsilon A_1(x, y) + \epsilon^2 A_2(x, y) + \dots \quad (17)$$

and

$$P = \epsilon^{-1} P_{-1}(x, y) + \epsilon P_1(x, y) + \epsilon^2 P_2(x, y) + \dots \quad (18)$$

From above, A_0 represents the adiabatic approximation, meaning the system remains in its instantaneous eigenstate whilst a perturbation is implemented, the higher orders correspond to the amplitude terms along the transverse wavefield. P is the phase of the wave expanded in terms of ϵ , it must be complex valued, as to ensure the WKBJ ansatz (16) includes all cases

of wave activity, ie propagating and decay. Note we can ignore an $O(\epsilon^0)$ term from equation (18) since it can be accounted for by the first term in equation (17). We now substitute the ansatz into (13) in the following way:

Using equation(17), we see that

$$\phi_x(x, y) = AP_x e^P + A_x e^P, \quad (19)$$

$$\text{and } \phi_{xx}(x, y) = AP_x^2 e^P + (AP_{xx} + P_x A_x) e^P + A_x P_x e^P + A_{xx} e^P, \quad (20)$$

and similarly

$$\phi_{yy}(x, y) = AP_y^2 e^P + (AP_{yy} + P_y A_y) e^P + A_y P_y e^P + A_{yy} e^P. \quad (21)$$

We now substitute (20), (21) and (16) into the Helmholtz equation and expand to obtain

$$\begin{aligned} & \epsilon^2 [AP_x^2 e^P + (AP_{xx} + P_x A_x) e^P + A_x P_x e^P + A_{xx} e^P] + \\ & [AP_y^2 e^P + (AP_{yy} + P_y A_y) e^P + A_y P_y e^P + A_{yy} e^P] + [k^2 A e^P] = 0 \end{aligned}$$

Cancelling a factor of e^P then gives

$$\epsilon^2 [AP_x^2 + (AP_{xx} + P_x A_x) + A_x P_x + A_{xx}] + [AP_y^2 + (AP_{yy} + P_y A_y) + A_y P_y + A_{yy}] + k^2 A = 0. \quad (22)$$

Now substituting(17) and (18) into(22) and expand for small ϵ , we find that.

$$\begin{aligned}
& \epsilon^2[(A_0 + \epsilon A_1 + \epsilon^2 A_2 + \dots)(\epsilon^{-2} P_{-1x}^2 + 2P_{-1x} P_{1x} + \epsilon P_{2x} + \epsilon^2 P_{1x}^2 + \epsilon^3 P_{1x} P_{2x} + \dots)] \\
& \quad + (A_0 + \epsilon A_1 + \epsilon^2 A_2 + \dots)(\epsilon^{-1} P_{-1xx} + \epsilon_1 P_{1xx} + \epsilon^2 P_{2xx} + \dots) \\
& + 2[(A_{0x} + \epsilon A_{1x} + \epsilon^2 A_{2x} + \dots)(\epsilon^{-1} P_{-1x} + \epsilon_1 P_{1x} + \epsilon^2 P_{2x} + \dots) + (A_{0xx} + \epsilon A_{1xx} + \epsilon^2 A_{2xx} + \dots)] \\
& \quad + [(A_0 + \epsilon A_1 + \epsilon^2 A_2 + \dots)(\epsilon^{-2} P_{-1y}^2 + 2P_{-1y} P_{1y} + \epsilon P_{2y} + \epsilon^2 P_{1y}^2 + \epsilon^3 P_{1y} P_{2y} \dots)] \\
& \quad + (A_0 + \epsilon A_1 + \epsilon^2 A_2 + \dots)(\epsilon^{-1} P_{-1yy} + \epsilon_1 P_{1yy} + \epsilon^2 P_{2yy} + \dots) \\
& + 2[(A_{0y} + \epsilon A_{1y} + \epsilon^2 A_{2y} + \dots)(\epsilon^{-1} P_{-1y} + \epsilon_1 P_{1y} + \epsilon^2 P_{2y} + \dots) + (A_{0yy} + \epsilon A_{1yy} + \epsilon^2 A_{2yy} + \dots)] \\
& \quad + k^2(A_0 + \epsilon A_1 + \epsilon^2 A_2 + \dots) = 0
\end{aligned}$$

Now we compare coefficients of ϵ . The $O(\epsilon^{-2})$ term are

$$A_0 P_{-1y}^2 = 0 \text{ and therefore } P_{-1y} = 0 \text{ which implies that } P_{-1} = f(x)$$

where $f(x)$ is an unknown function, to be determined later. At order ϵ^{-1} we find that

$$A_0 P_{-1yy}^2 + A_{0y} P_{-1y} = 0, \tag{23}$$

is trivially satisfied, since from (23), $P_{-1y} = P_{-1yy} = 0$. The $O(\epsilon^0)$ terms are

$$A_0 P_{-1x}^2 + A_{0yy} + A_0 k^2 + P_{-1y} P_{1y} = 0,$$

which simplify to

$$\begin{aligned}
& A_{0yy} + A_0 P_{-1x}^2 + A_0 k^2 = 0, \\
& \text{ie, } A_{0yy} + A_0 (P_{-1x}^2 + k^2) = 0.
\end{aligned} \tag{24}$$

If we now substitute $f(x)$ for P_{-1}

$$A_{0yy} + A_0(f'^2 + k^2) = 0$$

which is a second order differential equation with solution

$$A_0 = C_1 \cos(y\alpha(x)) + C_2 \sin(y\alpha(x)), \quad (25)$$

where $\alpha^2(x) = f'^2 + k^2$ and $C_1 = C_1(x), C_2 = C_2(x)$. Using the Dirichlet conditions, the solution is

$$A_0 = C_3 \sin((y + h_-)\alpha(x)), \quad (26)$$

for $C_3 = C_3(x)$. Then either $C_3 = 0$ leading to a trivial solution or $\alpha(x)(h_+ + h_-) = n\pi$. We have $A_0 = a_0(x)S(x, y)$ where $S(x, y) = C_3 \sin(\alpha(x)(h_+ + h_-))$, and $\alpha_n(x) = \frac{n\pi}{w(x)}$ for repeated solutions of the sin function, $n = 1, 2, \dots$, $w(x) = [h_+(x) + h_-(x)]$ and $a_0(x)$, is a function of x we later calculate. Firstly, we normalise the function of $S(x, y)$ in order to find the value for C_3 .

$$\int_{-h_-}^{h_+} C_3^2 \sin^2(\alpha(x)y + h_-) dy = 1 \quad (27)$$

Using a trigonometric identity, we separate the terms,

$$\int_{-h_-}^{h_+} \frac{C_3^2}{2} - \frac{C_3^2}{4n\pi} \sin \frac{(2n\pi(y + h_-))}{w(x)} dy = 1 \quad (28)$$

integrating and evaluating at the limits, the equation is thus

$$C_3^2(h_+(x) + h_-(x)) = 2 \quad (29)$$

rearranging appropriately we see

$$C_3 = \left(\frac{2}{(h_+(x) + h_-(x))} \right)^{\frac{1}{2}}. \quad (30)$$

Therefore

$$S(x, y) = \left(\frac{2}{(h_+(x) + h_-(x))} \right)^{\frac{1}{2}} \sin(\alpha(x)(y + h_-)) \quad (31)$$

We continue equating orders of ϵ . The $O(\epsilon^1)$ terms are

$$A_1 P_{-1x}^2 + A_0 P_{-1xx} + 2A_{0x} P_{-1x} + 2P_{1y} P_{1y} A_1 + A_0 P_{2y} + A_0 P_{1yy} + 2A_{0y} P_{1y} + A_{1yy} + k^2 A_1 = 0$$

Recalling that $P_{-1} = f(x)$ and the derivatives of this function, we implement this in the

equation above

$$\begin{aligned} A_{1yy} + A_1 P_{-1x}^2 + k^2 + A_0(f_n'' + P_{1yy}) + 2A_{0x}f_n' + 2A_{0y}P_{1y} &= 0 \\ \text{ie. } A_{1yy} + A_1(P_{-1x}^2 + k^2) &= -A_0(f_n'' + P_{1yy}) - 2A_{0x}f_n' - 2A_{0y}P_{1y}. \end{aligned} \quad (32)$$

Now multiply (32) by A_0 and integrate from $y = -h_-$ to $y = h_+$ which leads to

$$\int_{-h_-}^{h_+} [A_{1yy} + \alpha_n^2 A_1] A_0 dy = 0. \quad (33)$$

Integrating by parts, we see the integration evaluates to zero.

$$A_0 A_{1y} \Big|_{-h_-}^{h_+} + \left(- \int_{-h_-}^{h_+} A_{1y} A_{0y} dy + \alpha_n^2 \int_{-h_-}^{h_+} A_0 A_1 dy \right) = 0. \quad (34)$$

$$A_0 A_{1y} \Big|_{-h_-}^{h_+} - A_1 A_{0y} \Big|_{-h_-}^{h_+} + \int_{-h_-}^{h_+} A_{0yy} A_1 dy + \alpha_n^2 A_0 A_1 \Big|_{-h_-}^{h_+} - A_0 A_1 \Big|_{-h_-}^{h_+} = 0. \quad (35)$$

Since we know the function of A_0 we can evaluate at the limits, and see this is zero. Hence using this solvability condition on the right hand side equation,

$$\int_{-h_-}^{h_+} A_0 [A_0(f_n'' + P_{1yy}) + 2A_{0x}f_n' + 2A_{0y}P_{1y}] dy = 0. \quad (36)$$

Taking the differentiation under the integral sign, ie. $\frac{d}{dx} F(x) = f(x, b(x))b'(x) - f(x, a(x))a'(x) + \int_{a(x)}^{b(x)} \frac{\partial}{\partial x} f(x, t) dt$ where $F(x) = \int_{a(x)}^{b(x)} f(x, t) dt$. Applying it to equation (36), we see that due to the limits, $\int_{-h_-}^{h_+} (A_0^2 P_{1yy} + 2A_0 A_{0y} P_{1y}) dy$ evaluates to zero, leaving

$$\int_{-h_-}^{h_+} \frac{\partial}{\partial x} (A_0^2 f_n'' + 2f_n' A_{0x} A_0) dy = 0 \quad (37)$$

This reduces to,

$$\int_{-h_-}^{h_+} \frac{\partial}{\partial x} (f_n' A_0^2) dy = 0. \quad (38)$$

Then by rules of differentiation under the integral sign, we are able to interchange the two functions, such that

$$\frac{d}{dx} \left(\int_{-h_-}^{h_+} (f_n' A_0^2) dy \right) = 0 \quad (39)$$

f' is a function of x so taking it out of the integrand, we let $a_0^2 = \int_{-h_-}^{h_+} A_0^2 dy$, since $\int_{-h_-}^{h_+} A_0^2 dy =$

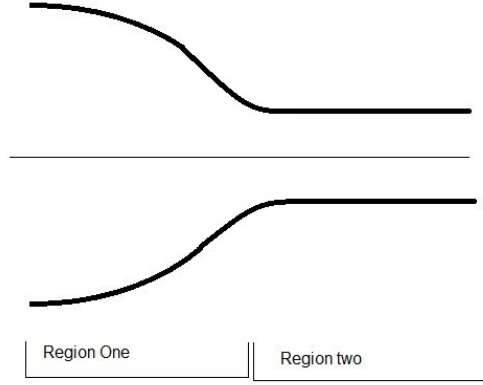


Figure 2: Diagram illustrating a tapered duct

$\int_{-h_-}^{h_+} a_0^2 S_n^2(x, y) dy$ such that equation (39) reduces to

$$\frac{d}{dx}(f'_n a_0^2) = 0. \quad (40)$$

Integrating both sides we find, $a_0(x) = C_4 |f'_n|^{-\frac{1}{2}}$, for some constant C_4 .

To solve for f we must firstly consider two cases for $\alpha^2(x) - k^2 \geq 0$ and $\alpha^2(x) - k^2 \leq 0$:

$$f(x) \equiv f_n = \begin{cases} \pm i \int^x (k^2 - \alpha_n^2(x_0))^{\frac{1}{2}} dx_0, & k \geq \alpha_n(x) \\ \pm i \int^x (\alpha_n^2(x_0) - k^2)^{\frac{1}{2}} dx_0, & k \leq \alpha_n(x) \end{cases} \quad (41)$$

This defines the two cases of the problem. When the wavenumber k is larger than the cut-off frequency $\alpha_n(x)$, then the trapped mode is propagating.

If however the wavenumber k is smaller than the cut-off frequency, then the trapped mode is evanescent.

This leads to the final solution

$$\phi(x, y) = C_n |f'_n|^{\frac{1}{2}} S_n(x, y) \exp\{\epsilon^{-1} f_n\} + O(\epsilon) \quad (42)$$

2.3 The Reflective Wave in a Tapered Duct

Consider a tapered duct

Figure (2) illustrates two regions labelled on the tapered duct, the first region, allows a

travelling wave to oscillate, passing through to the tapered region we have labelled region two. In this region the wave is evanescent and hence will exponentially decay. We find the incoming wave mostly reflecting back into region one while only a fraction of the wave transmits into the tapered region.

By using the turning point analysis, we can calculate the transmission and reflection coefficients of the n -th mode accordingly. We find that we have a two case solution for the n -th mode. The first, when the mode propagates in $x \leq x_n$ [region one], where x_n denotes the value of x at the n -th mode.

$$\phi_n = \phi_n^{(-)}(x)S_n(x, y), \quad (43)$$

where

$$\phi_n^{(-)} = \frac{I \exp\{-i\epsilon^{-1} \int_x^{x_n} (k^2 - \alpha_n^2(x_0))^{\frac{1}{2}} dx_0\} + R_n \exp\{i\epsilon^{-1} \int_x^{x_n} (k^2 - \alpha_n^2(x_0))^{\frac{1}{2}} dx_0\}}{(k^2 - \alpha_n^2(x))^{\frac{1}{4}}} \quad (44)$$

I is the amplitude of the incident wave and R_n is the reflection coefficient.

The second case, is when the mode is evanescent in $x \geq x_n$ [region two]

$$\phi_n = \phi_n^{(+)}(x)S_n(x, y), \quad (45)$$

$$\phi_n^{(+)} = \frac{T_n \exp -\epsilon^{-1} \int_{x_n}^x (\alpha_n^2(x_0) - k^2)^{\frac{1}{2}} dx_0}{(k^2 - \alpha_n^2(x))^{\frac{1}{4}}} \quad (46)$$

T_n is the transmission coefficient. Note also, due to the conservation of energy, because the wave decays when transmitted, all the energy is reflected back, therefore $|R_n| = |I|$.

However this condition is not valid in a small neighbourhood of $x = x_0$. Therefore in order to examine this small region we must consider $k^2 - \alpha_n^2(x_0) = -\Delta_n(x_0 - x_n) + O((x_0 - x_n)^2)$, where $\Delta_n = \frac{-2k^3 w'(x_n)}{(n\pi)}$.

We then see that

$$\exp(i\epsilon^{-1} \int_x^{x_n} (k^2 - \alpha_n^2(x_0))^{\frac{1}{2}} dx_0) \sim \exp(\epsilon^{-1} \int_x^{x_n} (x_n - x_0)^{\frac{1}{2}} dx_0), \quad (47)$$

$$= \exp(i\frac{2}{3}\epsilon^{-1}\Delta_n^{\frac{1}{2}}(x_n - x_0)^{\frac{3}{2}}), \quad (48)$$

so that, in the limit $x_0 \rightarrow x_n^{(-)}$ there is a non-uniformity when $(x_n - x_0)^{\frac{3}{2}} = O(\epsilon)$. Similarly for the evanescent case in the limit $x_0 \rightarrow x_n^{(+)}$, we have

$$\exp\left(-\epsilon^{-1} \int_{x_n}^x (\alpha_n^2(x_0) - k^2)^{\frac{1}{2}} dx_0\right) = \exp\left(-\frac{2}{3}\epsilon^{-1} \Delta_n^{\frac{1}{2}} (x_0 - x_n)^{\frac{3}{2}}\right), \quad (49)$$

so again there is a non-uniformity when $(x_0 - x_n)^{\frac{3}{2}} = O(\epsilon)$. We can now utilise this knowledge in our governing equation, by setting $\phi_n(x, y) = \chi_n(\eta)S_n(x, y)$, where $\eta = \epsilon^{-\frac{2}{3}}(x_0 - x_n)$ is $O(1)$ in the region of interest. Now

$$\phi_x = \chi_n' \eta_x S_n + \chi_n \frac{\partial S_n}{\partial x} = \epsilon^{-\frac{2}{3}} \chi_n' S_n + \chi_n \frac{\partial S_n}{\partial x}. \quad (50)$$

Differentiating again we have

$$\phi_{xx} = \epsilon^{-\frac{4}{3}} \chi_n'' S_n + 2\epsilon^{-\frac{2}{3}} \chi_n' \frac{\partial S_n}{\partial x} + \chi_n \frac{\partial^2 S_n}{\partial x^2} \text{ so that} \quad (51)$$

$$\epsilon^2 \phi_{xx} = \epsilon^{\frac{2}{3}} \chi_n'' S_n + 2\epsilon^{\frac{4}{3}} \chi_n' \frac{\partial S_n}{\partial x} + O(\epsilon^2) \quad (52)$$

$$\text{lastly } \phi_{yy} = \chi_n S_n \alpha_n^2(x) \quad (53)$$

since as previously stated $S_n(x, y) = (2/w)^{\frac{1}{2}} \sin[\alpha_n(y - h_-)]$. Finally the last term of the Helmholtz equation

$$k^2 \phi = k^2 \chi_n S_n. \quad (54)$$

Simplifying and combining the three terms of the Helmholtz equation, we see that

$$\epsilon^{\frac{2}{3}} \chi_n'' S_n + 2\epsilon^{\frac{4}{3}} \chi_n' \frac{\partial S_n}{\partial x} + O(\epsilon^2) + \chi_n S_n (k^2 - \alpha_n^2(x)) = 0 \quad (55)$$

But $k^2 - \alpha_n^2(x) = -\Delta_n(x - x_n) + O(x - x_n)^2$, so equation(55) becomes

$$\epsilon^{\frac{2}{3}} \chi_n'' S_n + 2\epsilon^{\frac{4}{3}} \chi_n' \frac{\partial S_n}{\partial x} + O(\epsilon^2) - \chi_n S_n \Delta_n (x - x_n) = 0. \quad (56)$$

Now in equation (56) $S_n = S_n(x, y)$ and similarly for S_{n_x} by using the Taylor series expansion, $f(x) = f(x_n) + (x - x_n)f_x(x_n) + \frac{1}{2}(x - x_n)^2 f_{xx}(x_n) + O((x - x_n)^3)$, expand in the following way:

$$\epsilon^{\frac{2}{3}} \chi_n'' S_n(x, y) + 2\epsilon^{\frac{4}{3}} \chi_n' S_{n_x}(x, y) - \chi_n S_n(x, y) \Delta_n \epsilon^{\frac{2}{3}} \eta + O(\epsilon^2) = 0 \quad (57)$$

But $x = x_n + \epsilon^{\frac{2}{3}}\eta$, so $f(x) = f(x_n) + \epsilon^{\frac{2}{3}}\eta f'(x_n) + \frac{1}{2}\epsilon^{\frac{4}{3}}\eta^2 f''(x_n) + O(\epsilon^2)$

Hence equation (57)

$$\epsilon^{\frac{2}{3}}\chi_n''S_n(xn, y) + \epsilon^{\frac{2}{3}}\eta S_{n_x}(x, y) + O(\epsilon^{\frac{4}{3}}) + 2\epsilon^{\frac{4}{3}}\chi_n' \{S_{n_x}(x_n, y) + O(\epsilon^{\frac{2}{3}})\} - \chi_n \Delta_n \epsilon^{\frac{2}{3}}\eta \{S_n(x_n, y) + O(\epsilon^{\frac{2}{3}})\} + O(\epsilon^2) = 0 \quad (58)$$

We can rearrange, such that

$$\epsilon^{\frac{2}{3}}(\chi_n'' - \Delta_n \eta \chi_n) S_n = \epsilon^{\frac{4}{3}}(\chi_n'' + 2\chi_n' - \Delta_n \eta^2 \chi_n) \frac{\partial S_n}{\partial x}(x_n) + O(\epsilon^2).$$

Taking the leading order $\chi_n \approx \chi_n^{(0)}$ where

$$\chi_n^{(0)''} - \Delta_n \eta \chi_n = 0$$

This differential equation is of the form of an Airy equation, and hence the solution may be written in term of the Airy functions,

$$\chi_n^{(0)} = F_n \text{Ai}(\Delta_n^{\frac{1}{3}}\eta) + F_{2_n} \text{Bi}(\Delta_n^{\frac{1}{3}}\eta),$$

where Ai and Bi are the Airy's function of the first and second kind respectively and F_n and F_{2_n} are constants. Since the solution is bounded and decreases exponentially in the positive limit equation (49), then the Airy's function of the second kind is not part of the solution. Hence

$$\chi_n^{(0)} = F_n \text{Ai}(\Delta_n^{\frac{1}{3}}\eta),$$

where F_n is some constant. So the solution in the neighbourhood $x = x_0$ is

$$\phi \sim F_n \text{Ai}(\epsilon^{-\frac{2}{3}}\Delta_n^{\frac{1}{3}}(x - x_n)) S_n(x, y) \quad (59)$$

We can determine the constants R_n, T_n and F_n by comparing the expansions of ϕ across the boundary layer centered at $x = x_n$ with the the standard argument form of the Airy function in the inner region given below:

$$\phi_n \sim F_n \pi^{-\frac{1}{2}} \Delta_n^{-\frac{1}{12}} (-\eta)^{-\frac{1}{4}} \sin\left(\frac{\pi}{4} + \frac{2}{3}\Delta_n^{-\frac{1}{12}}(-\eta)\right) \quad (60)$$

$$\text{as } \eta \rightarrow -\infty \quad (61)$$

Firstly consider the limit in the negative direction:

$$\phi_n \sim \frac{F_n [\exp\{i(\frac{2}{3}\Delta_n^{\frac{1}{2}}(-\eta)^{\frac{3}{2}} + \frac{\pi}{4})\} - \exp\{-i(\frac{2}{3}\Delta_n^{\frac{1}{2}}(-\eta)^{\frac{3}{2}} + \frac{\pi}{4})\}]}{2i\pi^{\frac{1}{2}}\Delta_n^{\frac{1}{2}}(-\eta)^{\frac{1}{4}}}. \quad (62)$$

Compare with the expansion of equation (44)

$$\phi_n^- \sim \frac{I \exp\{-i\frac{2}{3}\Delta_n^{\frac{1}{2}}(-\eta)^{\frac{3}{2}}\} + R_n \exp\{i\frac{2}{3}\Delta_n^{\frac{1}{2}}(-\eta)^{\frac{3}{2}}\}}{\Delta_n^{\frac{1}{4}}\epsilon^{\frac{1}{2}}(-\eta)^{\frac{1}{4}}}. \quad (63)$$

We see that

$$\frac{I \exp\{-i(\frac{2}{3}\Delta_n^{\frac{1}{2}}(-\eta)^{\frac{3}{2}})\}}{\Delta_n^{\frac{1}{4}}\epsilon^{\frac{1}{2}}(-\eta)^{\frac{1}{4}}} = -\frac{iF_n \exp\{-i(\frac{2}{3}\Delta_n^{\frac{1}{2}}(-\eta) + \frac{\pi}{4})\}}{\Delta_n^{\frac{1}{12}}(-\eta)^{\frac{1}{4}}2\pi^{\frac{1}{2}}}, \quad (64)$$

only if

$$\frac{2\sqrt{\pi}I \exp i(\frac{\pi}{4})}{\Delta_n^{\frac{1}{6}}\epsilon^{\frac{1}{6}}} = -iF_n. \quad (65)$$

Similarly we see that

$$\frac{R_n \exp(i\frac{2}{3}\Delta_n^{\frac{1}{2}}(-\eta)^{\frac{3}{2}})}{\Delta_n^{\frac{1}{4}}\epsilon^{\frac{1}{6}}(-\eta)^{\frac{1}{4}}} = \frac{F_n \exp\{i\frac{2}{3}\Delta_n^{\frac{1}{2}}(-\eta) + \frac{\pi}{4}\}}{\Delta_n^{\frac{1}{12}}(\eta)^{\frac{1}{4}}2\pi^{\frac{1}{2}}}, \quad (66)$$

provided

$$\frac{2\sqrt{\pi}R_n \exp i\frac{\pi}{4}}{\Delta_n^{\frac{1}{4}}\epsilon^{\frac{1}{6}}(-\eta)^{\frac{1}{4}}} = iF_n. \quad (67)$$

Again for the limit tending in the positive direction, we compare both expansions:

$$\phi_n^+ \sim \frac{T_n \exp(-\frac{2}{3}\Delta_n^{\frac{1}{2}}\eta^{\frac{3}{2}})}{\Delta_n^{\frac{1}{4}}\epsilon^{\frac{1}{6}}\eta^{\frac{1}{4}}} \quad (68)$$

such that

$$T_n = \frac{1}{2}F_n\pi^{-\frac{1}{2}}\Delta_n^{\frac{1}{6}}\epsilon^{\frac{1}{6}}. \quad (69)$$

The solutions to equations (44) and (46) are given with the conditions of R_n , F_n and T_n being satisfied for a propagating ($x \leq x_n$) or evanescent wave ($x \geq x_n$).

2.4 A Uniform Expansion for a reflecting wave in a tapered duct

The analytical solution, is a composite of the inner boundary layer solution in the neighbourhood $x = x_0$ and of the outer slowly varying solution. It is therefore uniformly valid

throughout the duct, hence we are able to construct an expansion of the form,

$$\phi(x, y) = B(x, y)\text{Ai}(\epsilon^{\frac{2}{3}}g(x)) + C(x, y)\text{Ai}'(\epsilon^{\frac{2}{3}}g(x)), \quad (70)$$

where

$$B = B_0 + \epsilon^{\frac{2}{3}}B_1 + \epsilon^{\frac{4}{3}}B_2 + \dots \quad (71)$$

$$C = \epsilon^{\frac{2}{3}}C_1 + \epsilon^{\frac{4}{3}}C_2 + \dots \quad (72)$$

$$g = g_0 + \epsilon^{\frac{2}{3}}g_1 + \epsilon^{\frac{4}{3}}g_2 + \dots \quad (73)$$

$$(74)$$

The constant term in the expansion of C is not included, as we know from equation (59) the bounded solution includes only the Airy function and not the first derivative. Now we substitute these equations into the Helmholtz equation once again, and expand to obtain

$$\begin{aligned} \epsilon^2\phi_{xx} = & \epsilon^2B_{xx}\text{Ai} + 2B_x\text{Ai}'(\epsilon^{\frac{2}{3}}g)g'\epsilon^{\frac{4}{3}} + B\text{Ai}''(\epsilon^{\frac{2}{3}}g)g'^2\epsilon^{\frac{8}{3}} + B\text{Ai}'(\epsilon^{\frac{2}{3}}g)g''\epsilon^{\frac{4}{3}} \\ & + \epsilon^2C_{xx}\text{Ai}'(\epsilon^{\frac{2}{3}}g) + 2C_x\text{Ai}''(\epsilon^{\frac{2}{3}}g)g'\epsilon^{\frac{4}{3}} + C\text{Ai}'''(\epsilon^{\frac{2}{3}}g)g'^2\epsilon^{\frac{4}{3}} \end{aligned} \quad (75)$$

$$\phi_{yy} = B_{yy}\text{Ai}(\epsilon^{\frac{2}{3}}g(x)) + C_{yy}\text{Ai}'(\epsilon^{\frac{2}{3}}g(x)) \quad (76)$$

$$k^2\phi = B\text{Ai} + C\text{Ai}' \quad (77)$$

Now collecting terms of Airy functions of the first order

$$\epsilon^2B_{xx} + (k^2 + gg'^2)B + B_{yy} + \epsilon^{\frac{2}{3}}(g'^2C + gg''C + 2gg'C_x) = 0 \quad (78)$$

We expand coefficients of B and C

$$\begin{aligned} & \epsilon^{\frac{10}{3}}B_{2xx} + \epsilon^{\frac{8}{3}}B_{1xx} + \epsilon^2B_{0x} + k^2(B_0 + B_1\epsilon^{\frac{2}{3}} + B_2\epsilon^{\frac{4}{3}}) \\ & + B_{0yy}\epsilon^{\frac{2}{3}}B_{1yy} + \epsilon^{\frac{4}{3}}B_{2yy} + g_0g_0'^2B_0 + g_1g_0'^2 + (2g_0g_1'g_0')B_0\epsilon^{23}g_0g_0'^2B_1\epsilon^{\frac{2}{3}} \\ & + [[g_2g_0'^2 + 2g_1g_1'g_0' + g_0(2g_2'g_0' + g_1'^2)]B_0 + (g_1g_0'^2 + 2g_0g_1'g_0')B_1 + g_0g_0'^2B_2] \\ & + \epsilon^{\frac{4}{3}}B_{0yy} + \epsilon^{\frac{2}{3}}B_{1yy} + \epsilon^{\frac{4}{3}}B_{2yy} + g_0'^2C_1\epsilon^{\frac{4}{3}} \\ & + g_0^2g_0''\epsilon^{\frac{2}{3}} + (2g_1g_0g_0'' + g_0^2g_1'')\epsilon^{\frac{4}{3}} + 2g_0^2g_0'\epsilon^{\frac{2}{3}} + (4g_1g_0g_0' + 2g_0^2g_{1x}')\epsilon^{\frac{4}{3}} = 0. \end{aligned} \quad (79)$$

Now we equate coefficients of each power of ϵ to zero. The $O(\epsilon^{(0)})$ terms are

$$\begin{aligned} g_0 g_0'^2 B_0 + k^2 B_0 + B_{0_{yy}} &= 0 \\ B_{0_{yy}} + B_0(k^2 + g_0 g_0'^2) &= 0 \end{aligned} \quad (80)$$

Let $\alpha_n^2(x) = (k^2 + g_0 g_0'^2)$, such that we have a simplified second order differential equation, very similar to the expression 25, we can deduce g_0 is related to function f_n

$$B_{0_{yy}} + B_0(\alpha^2) = 0. \quad (81)$$

The general solution

$$B_0 = b_1 \cos(\alpha_n(x)y) + b_2 \sin(\alpha_n(x)y) \quad (82)$$

Using the Dirichlet Condition,

$$B_0 = b_0(x)(b_3 \sin(\alpha_n(x)(y + h_-))), \quad (83)$$

where b_3 can be determined by normalising the function $B_0 = (b_3 \sin(\alpha_n(x)(y + h_-)))$. We find that $b_3 = \sqrt{\frac{2}{w(x)}}$, and as before $w(x) = (h_+ + h_-)$. Now since $\alpha_n^2 = k^2 + g_0 g_0'^2$ there is a clear relation to (41). We can find the solution of $g_0(x)$, by setting the function to be a solution of the form

$$g_0 = (C f_n)^\gamma \quad (84)$$

where f_n is defined by the equation (41), differentiating g_0 again, we see that

$$g_0' = \gamma C^\gamma f_n^{(\gamma-1)} f_n' \quad (85)$$

Substituting these equations into $\alpha_n(x)$

$$k^2 + (\gamma^2 C^{3\gamma} f_n^{(3\gamma-2)} f_n')^2 \quad (86)$$

Let the function $g_0 = 1$ in order to determine the values for γ and C . If we let $f_n^{3\gamma-2} = 1$, then we see that $\gamma = \frac{2}{3}$. If we now let $\gamma^2 C^{3\gamma} = 1$ it follows that $C = (\gamma^{-\frac{2}{3}})$.

Hence

$$g_0(x) = \left(\frac{3}{2} f_n^{\frac{2}{3}}\right) \quad (87)$$

If we consider a small neighbourhood, $x = x_n$, such that $\alpha_n(x_n) = k$ and that $w'(x) \leq 0$ then if $x \geq x_n$ we have $\alpha_n(x) \geq k$ such that $g_0(x) = \left(\frac{3}{2} f_n^{\frac{2}{3}}\right)$. If however, $x \leq x_n$ then $\alpha_n(x) \leq k$ hence $g_0(x) = \left(-\frac{3i}{2} f_n^{\frac{2}{3}}\right)$ a complex function. We require a real-valued function g ,

such that the solution takes the form,

$$g_0(x) = \begin{cases} -\left(\frac{3}{2} \int^x (k^2 - \alpha_n^2(x_0))^{\frac{1}{2}} dx_0\right)^{\frac{2}{3}}, & x \leq x_n \\ \left(\frac{3}{2} \int^x (\alpha_n^2(x_0) - k^2)^{\frac{1}{2}} dx_0\right)^{\frac{2}{3}}, & x \geq x_n \end{cases} \quad (88)$$

Continuing the order of equating coefficients of the airys function

$$\epsilon^{\frac{2}{3}} : k^2 B_1 + B_{1_{yy}} + (g_1 g_0'^2 + 2g_0 g_1' g_0') B_0 + g_0 g_0'^2 B_1 + g_0^2 g_0'' \quad (89)$$

And as before consider

$$B_{1_{yy}} + (k^2 + g_0 g_0'^2) B_1. \quad (90)$$

Let $k^2 + g_0 g_0'^2 = \alpha_n^2$ Multiplying equation (90) by B_0 and integrating from $y = -h_-$ to $y = -h_+$ the solution =0. Then by this solvability condition,

$$\int_{-h_-}^{h_+} g_0' (g_0' g_1 + 2g_0 g_1') B_0 dy = 0 \quad (91)$$

$$\int_{-h_-}^{h_+} [g_0'^2 g_1 + 2g_0 g_0' g_1'] B_0 dy = 0 \quad (92)$$

Then differentiating with respect to x,

$$\int_{-h_-}^{h_+} \frac{\partial}{\partial x} (g_0 g_1^2) dy \quad (93)$$

We can then reduce the equation further

$$\frac{d}{dx} (g_0 g_1^2) = 0 \quad (94)$$

Solving this first order differential, leads to the solution $g_1 = G|g_0|^{-\frac{1}{2}}$ Therefore $B_1 = b_1 S_n(x, y)$.

We will now consider the derivative of the Airy's function, and again, equate their coefficients.

$$\epsilon^2 C_{xx} + (k^2 + g g'^2) C + C_{yy} + \epsilon^{\frac{4}{3}} (g'' B + 2g' B_x) = 0 \quad (95)$$

Once again, we expand through B and C term,

$$\begin{aligned} & \epsilon^{\frac{8}{3}}C_{1_{xx}} + \epsilon^{\frac{10}{3}}C_{2_{xx}} + k^2(\epsilon^{\frac{2}{3}}C_1 + \epsilon^{\frac{4}{3}}C_2) + (\epsilon^{\frac{2}{3}}C_{1_{yy}} + \epsilon^{\frac{4}{3}}C_{2_{yy}}) + \\ & g_0g_0^{2'}C_1\epsilon^{\frac{2}{3}} + \epsilon^{\frac{4}{3}}g_0'B_0 + (g_{1''}B_0 + g_0'B_1)\epsilon^2 + (g_{2''}B_0 + g_{1''}B_1 + g_{0''}B_2)\epsilon^{\frac{8}{3}} \\ & +(g_{2''}B_1 + g_{1''}B_2)\epsilon^{\frac{10}{3}} + 2g_{0'}B_{0'}\epsilon^{\frac{4}{3}} + (2g_{2'}B_{0_x} + 2g_{2'}B_{2_x} + 2g_{0'}B_{2_x})\epsilon^{\frac{8}{3}} + \\ & (2g_{2'}B_{1_x} + 2g_{1'}B_{2_x})\epsilon^{\frac{10}{3}} + [(g_1g_0'^2 + 2g_0g_{1'}g_{0'}C_1 + g_0g_0'^2C_2)\epsilon^{\frac{4}{3}} = 0. \end{aligned}$$

We will now equate the coefficients of the derivative of the Airy functions. The order $\epsilon^{\frac{2}{3}}$ has the following terms,

$$C_{1_{yy}} + g_0g_0'^2C_1 + k^2C_1 = 0 \quad (96)$$

$$= C_{1_{yy}} + (g_0g_0'^2 + k^2)C_1 = 0 \quad (97)$$

Let

$$\alpha_n^2 = g_0g_0'^2 + k^2. \quad (98)$$

So that we now have,

$$C_{1_{yy}} + \alpha_n^2C_1 = 0. \quad (99)$$

This second order differential equation is solved, as in previous cases

$$C_1 = c_1(x)S_n(x, y), \quad (100)$$

such that $S_n(x, y)$ has been previously defined, and c_1 is some constant to be determined.

Continuing equating orders of ϵ :

$$\begin{aligned} & k^2C_2 + C_{2_{yy}} + g_0''B_0 + 2g_0'B_{0_x} + (g_1g_0'^2 + 2g_0g_1'g_0')C_1 \\ & + g_0g_0'C_2C_{2_{yy}} + (k^2 + g_0g_0'^2)C_2 + g_0''B_0 + 2g_0'B_{0_x} = 0 \end{aligned} \quad (101)$$

$$(102)$$

$$C_{2_{yy}} + \alpha^2C_2 = -2g_0'B_{0_x} - g_0''B_0 \quad (103)$$

By integrating the left hand side, we find this is zero, more importantly this shows the expansion of C as zero and hence we can consider the right hand side of the equation to

equal zero through the solvability condition, in order to find b_0 .

$$\int_{-h_-}^{h_+} B_0(2g'_0 B_{0,x} - g''_0 B_0) dy \quad (104)$$

This equation can be reduced such that

$$\int_{-h_-}^{h_+} \frac{\partial}{\partial x} g'_0 B_0^2 dy = 0 \quad (105)$$

Taking g'_0 out of the integrand, and substituting some constant $b_0 = \int_{-h_-}^{h_+} g'_0 dy$. This then becomes a first order differential equation,

$$\frac{d}{dx}(b_0^2 g'_0) \quad (106)$$

and takes the solution of the form,

$$b_0 = G_n |g'_0|^{-\frac{1}{2}} \quad (107)$$

where constant G_n is to be determined and g'_0 is a rearrangement of the equation (98) $g'_0 = |k^2 - \alpha_n^2|^{\frac{1}{2}} |g_0|^{-\frac{1}{2}}$.

The particular solution of the expanded form defined in (70) can be assembled, such that

$$\phi(x, y) = B_0 \text{Ai}(\epsilon^{\frac{2}{3}} g(x)) \quad (108)$$

where B_0 is defined in (83) and $g(x)$ defined in(116), substituting this in,

$$\phi(x, y) = \frac{G_n |g_0(x)|^{\frac{1}{4}} \text{Ai}(\epsilon^{\frac{2}{3}} g_0(x)) S_n(x, y)}{|k^2 - \alpha_n^2(x)|^{\frac{1}{4}}} \quad (109)$$

G_n , is determined through the matching of expansions between (44) and the above equation, ensuring that $x \rightarrow -\infty$, where R_n is now unknown. As we are considering the negative limit, we note that $k \geq \alpha_n$ and $g_0(x) \leq 0$, so that the Airy function in the negative limit is

$$\text{Ai}(\epsilon^{-\frac{2}{3}} g_0(x)) \sim \frac{\epsilon^{\frac{1}{6}} \sin(\frac{\pi}{4} + \epsilon^{-1} \int_x^{x_n} k^2 - \alpha_n^2(x_0) dx_0)}{\sqrt{\pi} (g_0(x))^{\frac{1}{4}}} \quad (110)$$

and thus

$$\frac{\phi_n}{S_n(x, y)} = \frac{-iG_n \epsilon^{\frac{1}{6}} [\exp i(\frac{\pi}{4} + \int_x^{x_n} k^2 - \alpha_n^2(x_0) dx_0)] - [\exp -i(\frac{\pi}{4} + \int_x^{x_n} k^2 - \alpha_n^2(x_0) dx_0)]}{2\sqrt{\pi}(k)^2 - \alpha_n^2} \quad (111)$$

We see that

$$iG_n = \frac{2\sqrt{\pi}R_n \exp -i\frac{\pi}{4}}{\epsilon^{\frac{1}{6}}} \quad (112)$$

and

$$-iG_n = \frac{2\sqrt{\pi}I \exp i\frac{\pi}{4}}{\epsilon^{\frac{1}{6}}} \quad (113)$$

2.5 Trapping of waves in a symmetric duct

Now that we have found the uniformly-valid approximation given by equation (111), which calculates the process of the transmitting wave decaying as $x \rightarrow \infty$ and of the reflecting wave as $x \rightarrow -\infty$ within a tapered duct.

We must now start to investigate their location. Suppose that $h'_\pm(0) = 0$ and that $h'_\pm(x) \leq 0$ for $x \geq 0$ such that we only consider half of an infinite duct. The maximum of the bulge is located at $x = 0$ illustrated by fig (2). By taking only half the infinite duct into consideration, we are able to find the trappings for symmetric and antisymmetric modes. Then by reflecting the results, since throughout we have considered a symmetric waveguide, we gain a complete illustration of trapped modes within the entire tapered duct.

Such trapped modes can be determined by specific wavenumbers k , such that $\phi_n(0, y) = 0$ for the anti-symmetric modes in x , and $\phi_{n_x}(0, y) = 0$ for the symmetric modes in x . These wavenumbers are determined in the range $-h_-(0) \leq y \leq -h_+(0)$ where ϕ_n is given by (111). Since $h'_\pm(0) = 0$, this implies $w'(0) = 0$, remembering $w(x) = [h_+(x) + h_-(x)]$ and since, $\alpha_n = \frac{n\pi}{w(x)}$ it follows that $\alpha'_n(0) = 0$. We therefore seek values of k , for which, $\text{Ai}(\epsilon^{-\frac{2}{3}}g_{0_n}(x; k)) = 0$ where we may take $x = 0$ we determine the antisymmetric and symmetric modes by finding k in the following equations,

$$\text{Ai}(\epsilon^{-\frac{2}{3}}g_{0_n}(x; k)) = 0 \quad \text{antisymmetric modes} \quad (114)$$

$$\text{Ai}'(\epsilon^{-\frac{2}{3}}g_{0_n}(x; k)) = 0 \quad \text{symmetric modes} \quad (115)$$

where $g_{0_n}(x; k)$ is a slight variation from equation (88)

$$g_{0_n}(x; k) = \begin{cases} -(\frac{3}{2} \int_x^{\alpha_n^{-1}(k)} (k^2 - \alpha_n^2(x_0))^{\frac{1}{2}} dx_0)^{\frac{2}{3}}, & x \leq \alpha_n^{-1}(k) \\ (\frac{3}{2} \int_{\alpha_n^{-1}(k)}^x (\alpha_n^2(x_0) - k^2)^{\frac{1}{2}} dx_0)^{\frac{2}{3}}, & x \geq \alpha_n^{-1}(k) \end{cases} \quad (116)$$

as the limits are now between 0 and $\alpha_n^{-1}(k)$, where $\alpha_n^{-1}(k)$ is the unique positive root of $\alpha_n(\alpha_n^{-1}(k)) = k$ in the interval $(0, \infty)$. If we now denote the m -th root of $\text{Ai}(z) = 0$ by z_{-m} for $m \in \mathbb{N}$, such that the ordering of the roots are established as $z_{-(m+1)} \leq z_{-m}$, then approximations to wavenumbers k for the antisymmetric modes can be found by solving

$$\epsilon^{\frac{2}{3}} g_{0_n}(0; k) = z_m \text{ for } m, n \in \mathbb{N} \quad (117)$$

and for the symmetric case, by denoting z'_m as the m -th root at $\text{Ai}(z) = 0$ with the roots ordered $z'_{-(m+1)} \leq z'_{-m}$, the wavenumbers producing trapped modes are found via, the equation

$$\epsilon^{\frac{2}{3}} g_{0_n}(0; k) = z'_m \text{ for } m, n \in \mathbb{N} \quad (118)$$

Having found the specific wavenumbers to these trapped modes, we can implement the data into equation (116) in order to determine the structure of the waveguide. A Numerical solution, provides a clear graphical representation, of the results, as can be found in a later chapter of this paper.

3 The Neumann Problem

We will now consider the Neumann boundary condition, and compare the results to the Dirichlet.

$$\bar{\phi}_{xx} + \bar{\phi}_{yy} + k^2 \bar{\phi} = 0 \quad (-\infty < \bar{x} < \infty, \bar{y} = \pm \bar{h}_{\pm}(\bar{x})), \quad (119)$$

$$\bar{\phi}_{\zeta} = 0, \quad (-\infty < \bar{x} < \infty, \bar{y} = \pm \bar{h}_{\pm}(\bar{x})). \quad (120)$$

where ζ is the normal of the waveguide. The Neumann Case, follows a similar method to finding a solution as to the Dirichlet Problem. By non-dimensionalising the problem as before, substitute the given ansatz (16), (18) and (17), and expand the equation. Then by equating orders of ϵ we eventually get to the complementary function (25), where coefficients C_1 and C_2 are determined by the Neumann Boundary Condition (120). By differentiating (25), we see that the particular solution is $C_n(x, y) = C_3 \text{Cos}((y + h_-) * \alpha(x)) = 0$. We also require, when $y = h_+$

$$A'_0 = \alpha C_1 \cos(\alpha(h_+ + h_-)) = 0 \quad (121)$$

let $w(x) = (h_+ + h_-)$ then either $\alpha C_1 = 0$ which is trivial, or, $\alpha w = n\pi$ for $n \in \mathbb{N} \cup \{0\}$.

Thus the final solution is,

$$C_n(x, y) = C_3 \cos\left(\frac{n\pi}{w(x)}(y + h_-)\right) = 0, \quad (122)$$

for $n=0,1,2,\dots$. Again, we normalise the function to find C_3

$$C_n(x, y) = 1 \quad \text{for } n = 0 \quad (123)$$

$$C_n(x, y) = \sqrt{\frac{2}{w(x)}} \cos\left[\frac{n\pi}{w(x)}(y + h_-)\right] \quad \text{for } n = 1, 2, \dots \quad (124)$$

Reflecting the waves in the small neighbourhood, $x = x_n$ we substitute $\phi_n(x, y) = \chi_n(\eta)C_n(x, y)$ into the Helmholtz Equation, which leads to the same bounded solution as the Dirichlet case.

$$\chi_n^{(0)} = F_n \text{Ai}(\Delta_n^{\frac{1}{3}}\eta) \quad (125)$$

This gives the final solution of the ϕ equation:

$$\phi \sim F_n \text{Ai}(\epsilon^{\frac{2}{3}} \Delta_n^{\frac{1}{3}}(x - x_n)) C_n(x, y). \quad (126)$$

Then by comparing the Airy's standard argument with equations (44) and (46) we find a relation between F_n, R_n, T_n and I , by comparing the expansions of ϕ across the boundary layer centred at $x = x_n$ and taking the standard argument form of the Airy function given below:

$$\phi_n \sim F_n \pi^{-\frac{1}{2}} \Delta_n^{-\frac{1}{12}} (-\eta)^{-\frac{1}{4}} \cos\left(\frac{\pi}{4} + \frac{2}{3} \Delta_n^{-\frac{1}{12}} (-\eta)\right) \quad (127)$$

as $\eta \rightarrow -\infty$

Firstly consider (127) in terms of the exponential components, in order to compare with equation (44)

$$\phi_n \sim \frac{F_n \exp\{i(\frac{2}{3} \Delta_n^{\frac{1}{2}} (-\eta)^{\frac{3}{2}} + \frac{\pi}{4})\} + \exp\{-i(\frac{2}{3} \Delta_n^{\frac{1}{2}} (-\eta)^{\frac{3}{2}} + \frac{\pi}{4})\}}{2i\pi^{\frac{1}{2}} \Delta_n^{\frac{1}{12}} (-\eta)^{\frac{1}{4}}}. \quad (128)$$

As a reminder for the purpose of ease, we compare equation (44) given below

$$\phi_n^- \sim \frac{I \exp\{-i\frac{2}{3} \Delta_n^{\frac{1}{2}} (-\eta)^{\frac{3}{2}}\} + R_n \exp\{i\frac{2}{3} \Delta_n^{\frac{1}{2}} (-\eta)^{\frac{3}{2}}\}}{\Delta_n^{\frac{1}{2}} \epsilon^{\frac{1}{2}} (-\eta)^{\frac{1}{4}}}.$$

We see that

$$\frac{I \exp\{-i(\frac{2}{3}\Delta_n^{\frac{1}{2}}(-\eta)^{\frac{3}{2}})\}}{\Delta_n^{\frac{1}{4}}\epsilon^{\frac{1}{2}}(-\eta)^{\frac{1}{4}}} = \frac{iF_n \exp\{-i(\frac{2}{3}\Delta_n^{\frac{1}{2}}(-\eta) + \frac{\pi}{4})\}}{\Delta_n^{\frac{1}{2}}(-\eta)^{\frac{1}{4}}2\pi^{\frac{1}{2}}}, \quad (129)$$

only if

$$iF_n = \frac{2\sqrt{\pi}I \exp\{i(\frac{\pi}{4})\}}{\Delta_n^{\frac{1}{6}}\epsilon^{\frac{1}{6}}}. \quad (130)$$

$$iF_n = \frac{2\sqrt{\pi}R_n \exp\{-i(\frac{\pi}{4})\}}{\Delta_n^{\frac{1}{6}}\epsilon^{\frac{1}{6}}}, \quad (131)$$

and

$$F_n = \frac{2\sqrt{\pi}T_n}{\Delta_n^{\frac{1}{6}}\epsilon^{\frac{1}{6}}}. \quad (132)$$

As before we can derive a uniformly valid solution using the expansion

$$\phi(x, y) = B(x, y)\text{Ai}(\epsilon^{\frac{2}{3}}g(x)) + C(x, y)\text{Ai}'(\epsilon^{\frac{2}{3}}g(x)), \quad (133)$$

where $B(x, y), C(x, y)$ and $g(x)$ are defined in equations (71),(72),(73) respectively.

Substituting the ansatz into equation 13 and separating the terms of the Airy's equations, and of the first derivative of the Airy's equation. We then equate orders of ϵ . These terms, are replicated from the Dirichlet example, however the solution, varies from the sin function to the cos solution for the Neumann case. For example, in the equation (82), we use the Neumann condition instead, such that

$$B_0 = b_0(x)(b_3 \cos(\alpha_n(x)(y + h_-))), \quad (134)$$

Again, by normalising the function, we find $b_3 = \sqrt{\frac{2}{w(x)}}$, so that $B_0 = \sqrt{\frac{2}{w(x)}} \cos(\alpha_n(x)(y + h_-))$.
 $w(x) = (h_+ + h_-)$.

The equation for $g_0(x)$ still holds for the Neumann case, however again, $B_1 = b_1 C_n(x, y)$. Analysing the derivative of the Airy function the slight variation from the Dirichlet case, comes from the cos term thus, $C_1 = c_1 C_n(x, y)$, for some constant c_1 to be determined. This now gives rise to the solution of the uniform approximation to the n -th mode,

$$\phi(x, y) = \frac{G_n |g_0(x)|^{\frac{1}{4}} \text{Ai}(\epsilon^{\frac{2}{3}}g_0(x)) C_n(x, y)}{|k^2 - \alpha_n^2(x)|^{\frac{1}{4}}} \quad (135)$$

The G_n constant is found through matching of expansion, and as previously calculated, is a relation to R_n .

Having found the particular equation to solving the structure of reflecting and transmitting

waves within a tapered duct, bounded by a Neumann condition, we may now consider finding trapped modes. This again, is the same method for the Dirichlet case, hence it seems unnecessary to replicate chapter 2.5.

We may now begin to look at the Numerical approximations to this problem and determine the trappings for each case.

4 The Numerical Approach

4.1 Plotting solutions of k

The specific values of k are found by solving equations (117) and (118). Table 1 in the appendix shows a list of the first 24 solutions of the Airy function and the first derivative, denoted by Z_n and Z'_n for the antisymmetric and symmetric solutions respectively. Let us consider the trapped modes for the first antisymmetric solution, Z_1 , the program, developed through MATLAB, predicts the first two solutions of k using equation (118). To gain a better accuracy of the solution, the program was developed, such that it included a numerical technique, similar to the Euler Method. This involved finding subsequent values for wavenumber k through the given equation and improving this result by averaging the calculated value with a predicted value formed from the tangent of the two preceding values. This method was applied to the remaining Z_n solutions and the plotted result can be seen in figure (3).

This approach was also applied to the symmetric solutions as illustrated in figure (4). It is clear to see from figures (3) and (4), although not labelled, Z_1 (and Z'_1) are the lowest solutions plotted on both graphs, increasing up to Z_n or Z'_n .

The graphs illustrate the wavenumbers k , as a function of the bulge half width denoted h_1 , such that $2h_1$ is the maximum of the bulge (at $x = 0$) and $h_1 = 2$ at the limits $x \rightarrow \pm\infty$. Fixing $\epsilon = 0.1$ and the constant $G_n = 1$, we will compare solutions of k , for $n = 1$, where n is the multiple coefficient of π , in the $\alpha_n(x)$ equation. Figure (3) and (4) show the solutions of $\frac{k}{\pi}$ tending to 0.5 at the maximum of the bulge, which slowly decreases as we tend towards the cut-off frequency $x \rightarrow \pm\infty$. We would expect this, as this shows a decrease in existing trapped modes, in the given region.

It is important to mention that despite the improvement to the numerical technique used to get a more accurate solution at $h_1 = 1$, it was still difficult to get certain solutions of Z to a more accurate limit. This was because, at this region we were interpolating for asymptotic solutions.

We will now consider when $n = 2$, figures (5) and (6) illustrate the solutions of $\frac{k}{\pi}$ to be closer together, the gaps between Z_n and Z'_n solutions are less far apart than in figures

n=1 bulge.jpg

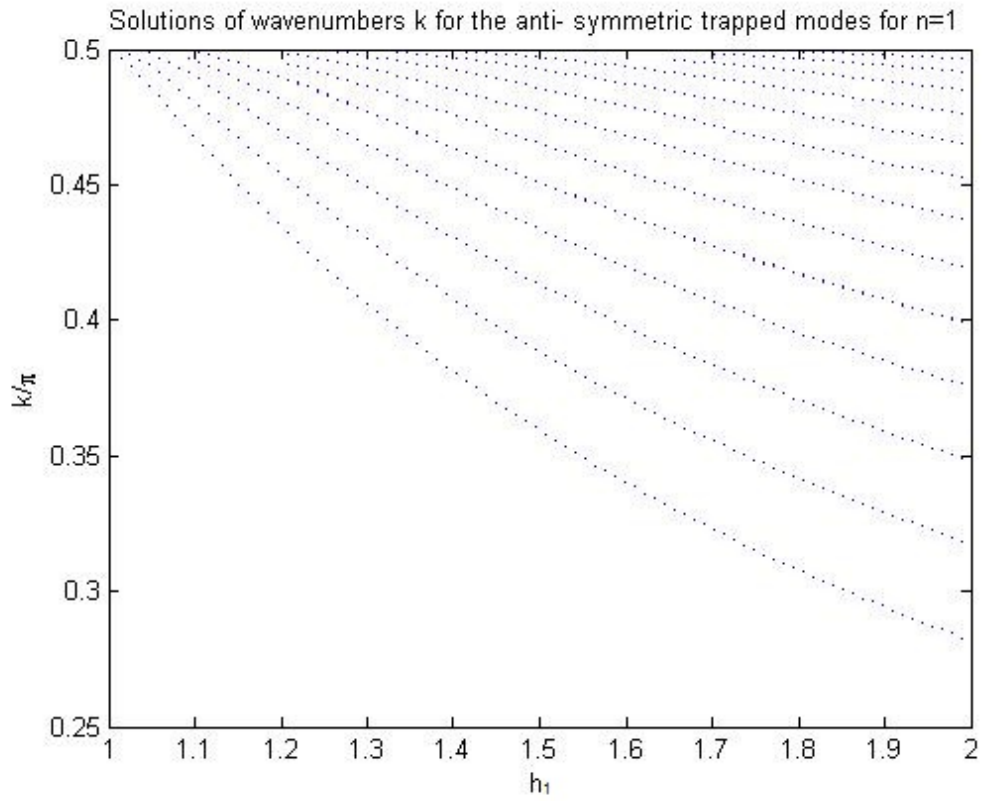


Figure 3: Solutions to wavenumbers of antisymmetric trapped modes for $n=1$ are plotted for each Airy solution, with the first solution Z_1 plotted as the lowest line increasing up to Z_n for $n=24$

n=1 bulge.jpg

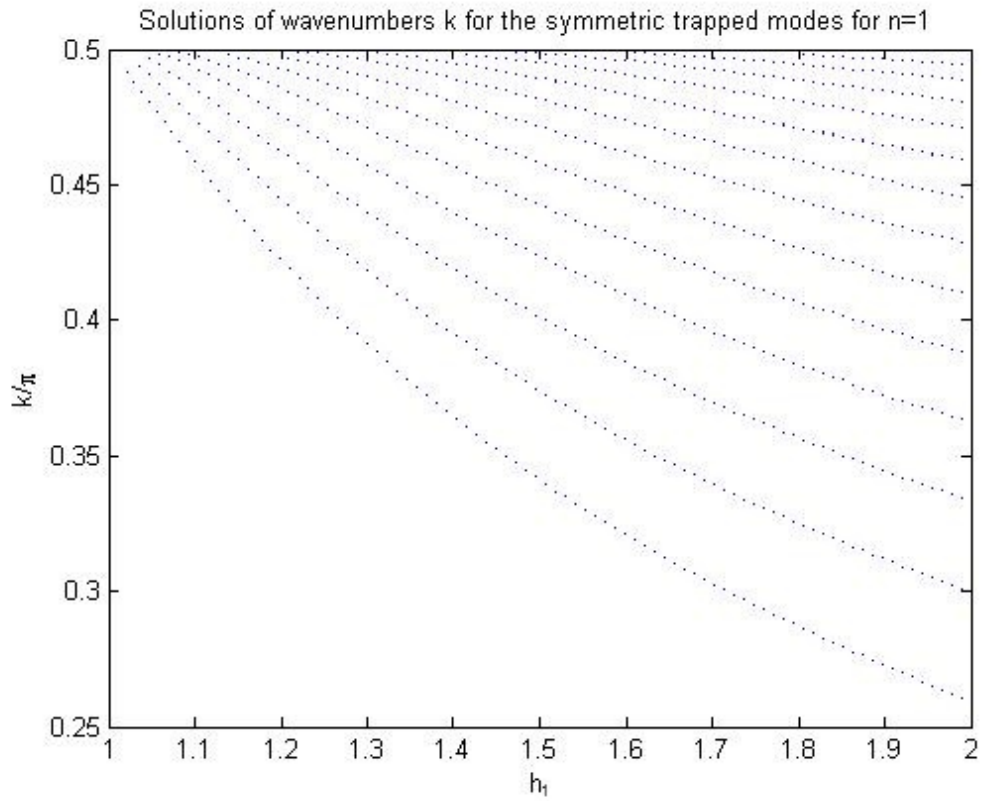


Figure 4: Solution to wavenumbers of symmetric trapped modes for $n=1$ are plotted for each Airy solution with the first solution Z'_1 plotted as the lowest line increasing up to Z_n for $n=24$

n=2 bulge.jpg

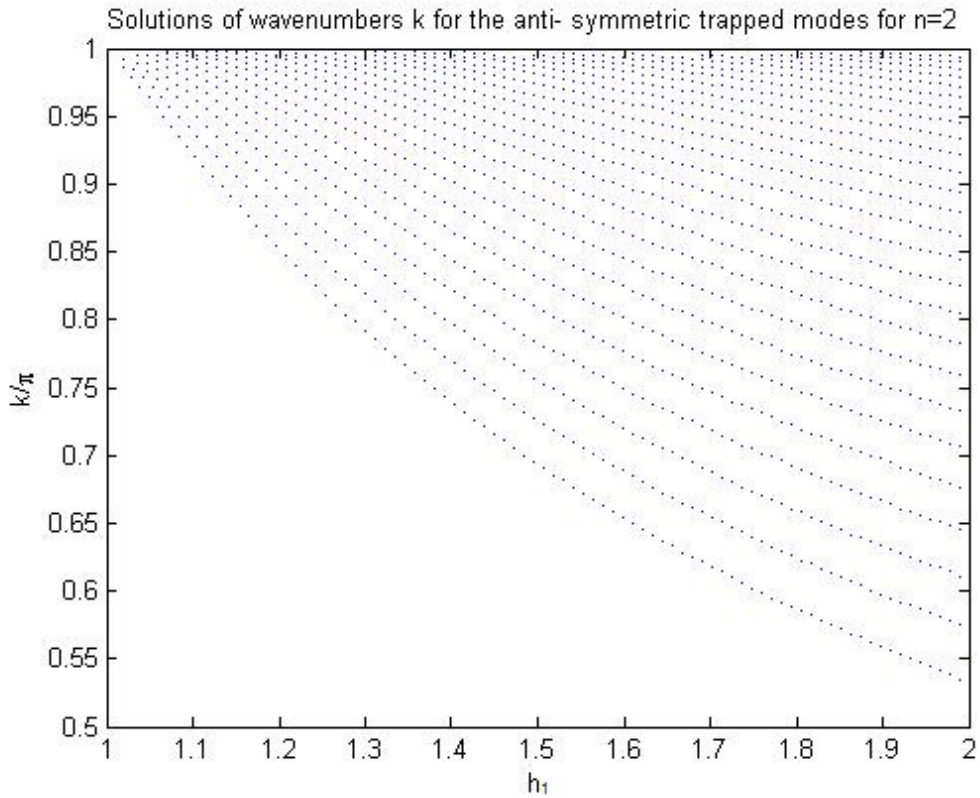


Figure 5: Wavenumbers of antisymmetric trapped modes for $n=2$.

(3) and (4). This shows an the existence of more trapped modes within the same region. Another difference, which may be obivous, is the values of $\frac{k}{\pi}$ tend to 1 as we are closer to the maximum of the bulge, and decays down to 0.5 as we near the cut-off. As we can see, by increasing n we increase the number of k solutions which in turn increases the number of trapped modes available.

n=2 bulge.jpg

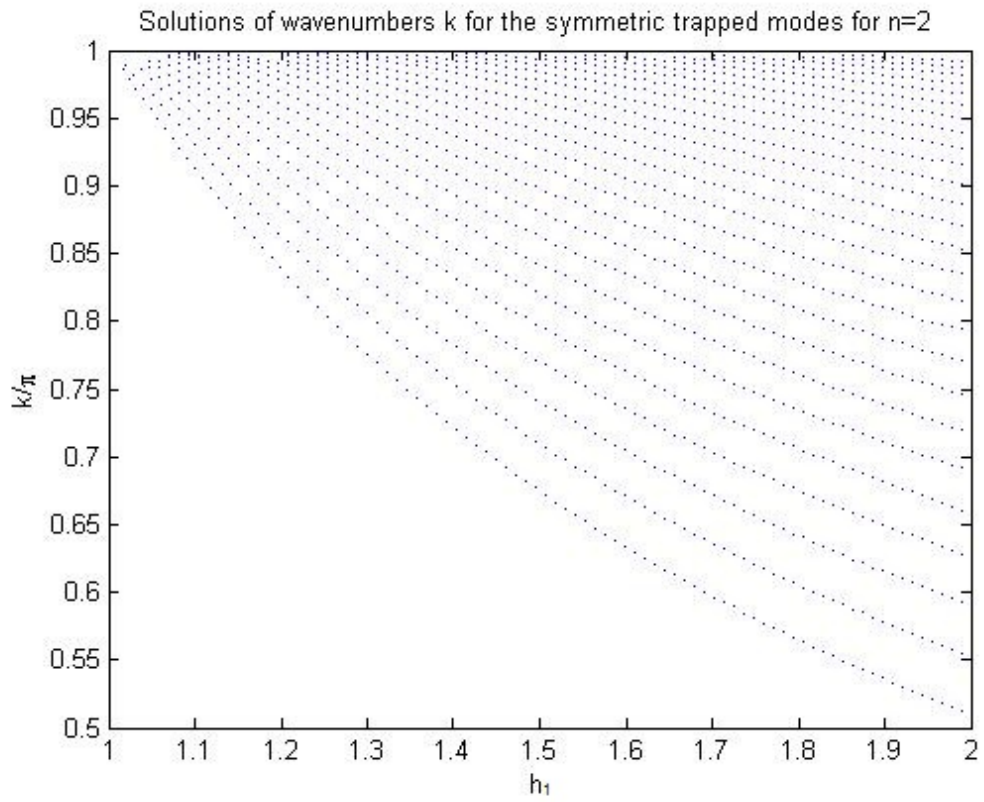


Figure 6: Wavenumbers of symmetric trapped modes for $n=2$.

bulge anti-symmetric n=1.jpg

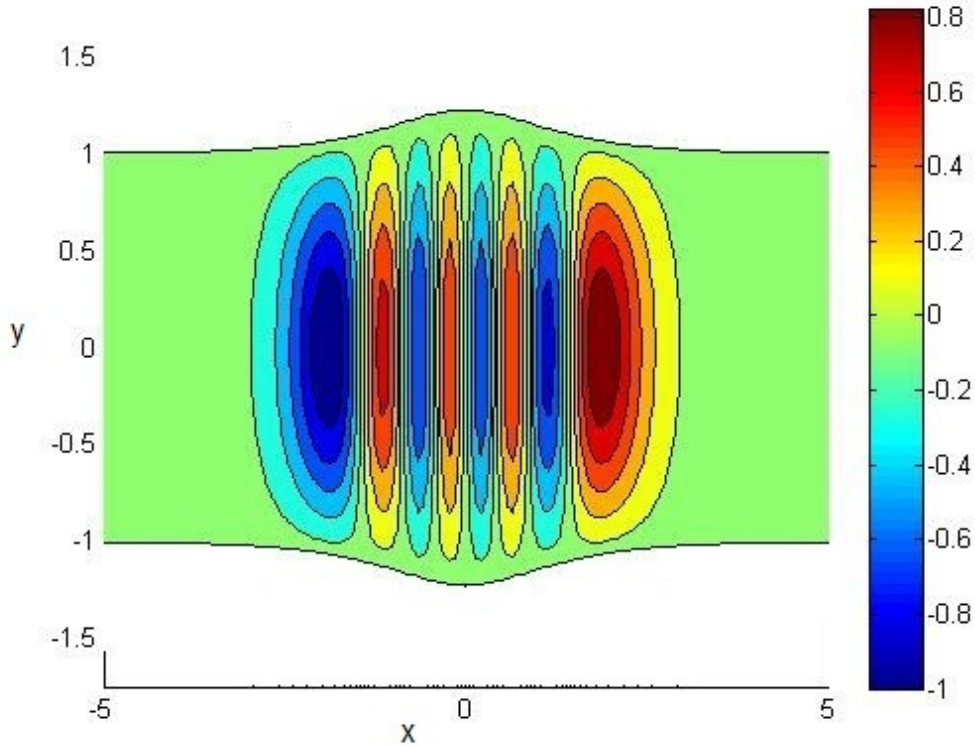


Figure 7: Contour plot of antisymmetric trapped modes.

4.2 Plotting the final solutions with Dirichlet boundary conditions

Once the values of k were found, we substituted them into the (109) and plotted the solutions, as shown in figures (7) and (8). The graphs illustrate one trapped mode propagating at the center of the bulge. Analysing figure (8), we can see at $x = 0$ the solution is reflected such that the complete solution is symmetric. For the antisymmetric case, figure (7), involved plotting the negative solutions of $\phi_n(x, y)$ against x and y .

A more visual representation of the trapped modes in the tapered duct can be viewed in figures (9) and (10). For the symmetric case it is very easy to see the symmetry at $x=0$, with large amplitudes near the cut-off frequency and small amplitudes at the centre. This suggest the resonance is at its largest at the cut-off regions, before it decays exponentially at $x \rightarrow \pm\infty$. The antisymmetric case is very similar, in that the resonant amplitude is at its maximum near the cut-off frequency for x in the positive limit, and its minimum amplitude near the cut-off for x in the negative limit. For an antisymmetric case, this is something we

bulge symmetric n=1.jpg

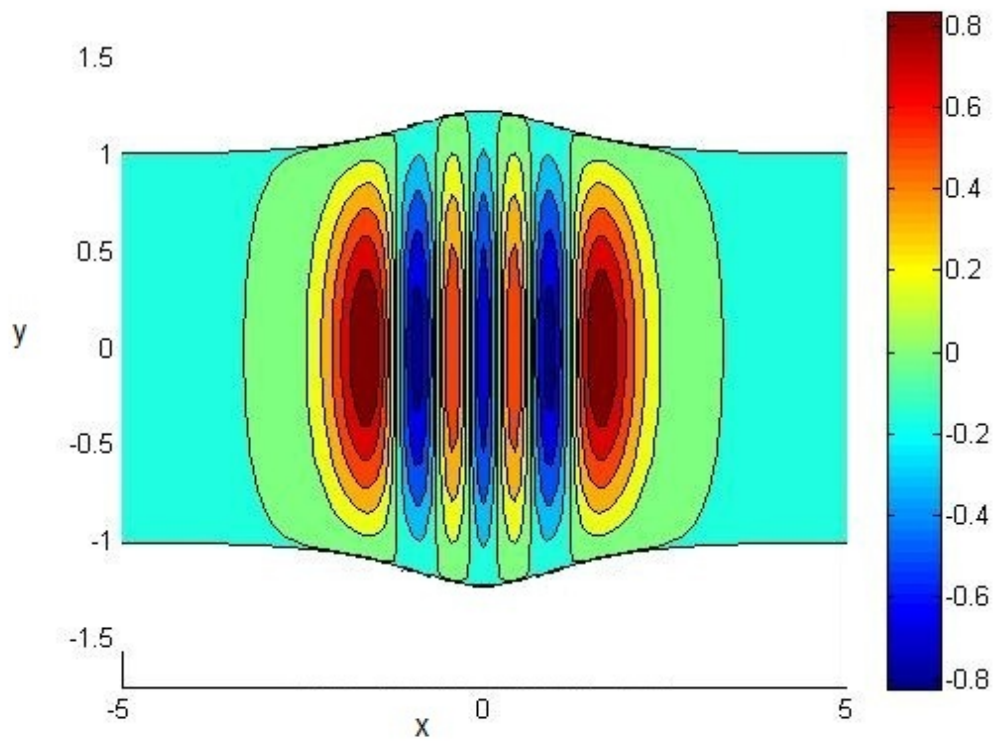


Figure 8: Contour plot of the symmetric trapped modes.

modes antisymmetric n=1.jpg

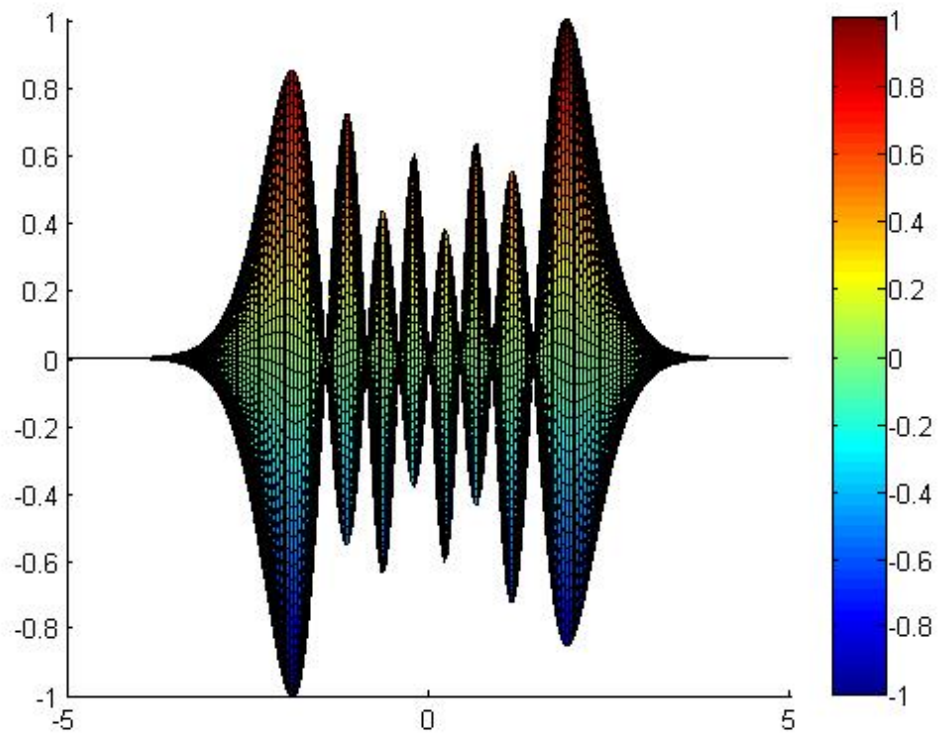


Figure 9: Surface plot of antisymmetric trapped modes, where we let $h_1 = 1.224$ and wavenumber $k = 1.500052$

modes symmetric n=1.jpg

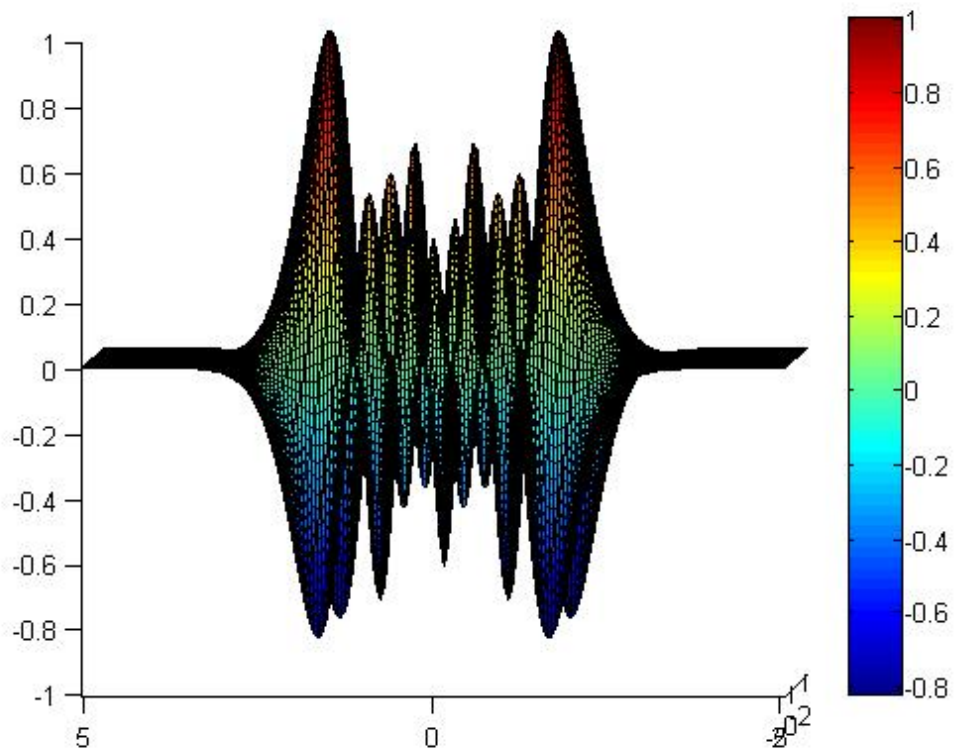


Figure 10: Surface plot of the symmetric trapped modes, where we let $h_1 = 1.224$ and wavenumber $k = 1.479089$

would expect.

bulge anti-symmetric n=2.jpg

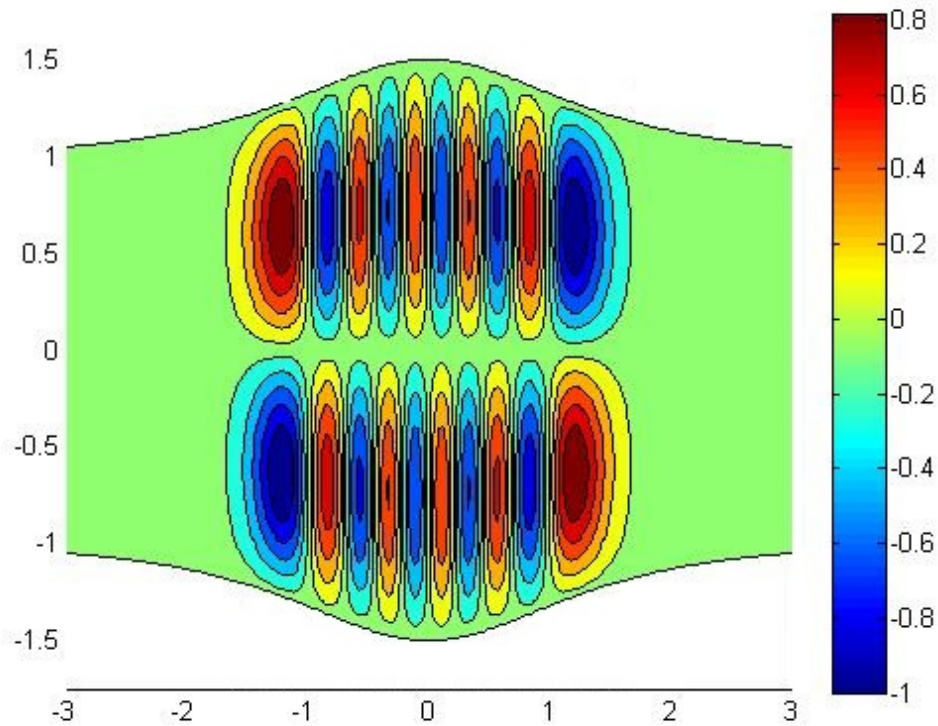


Figure 11: Contour plot of antisymmetric trapped modes for $n=2$.

Graphs (11) and (12) depict solutions of trapped modes for $n=2$. Both graphs illustrate the existence of two trapped modes, which we would expect, since by increasing n we are increasing the range of k and the number of Airy solutions available. Therefore we can deduce, increasing n leads to an increase in the number of possible trapped that could exist.

bulge symmetric n=2.jpg

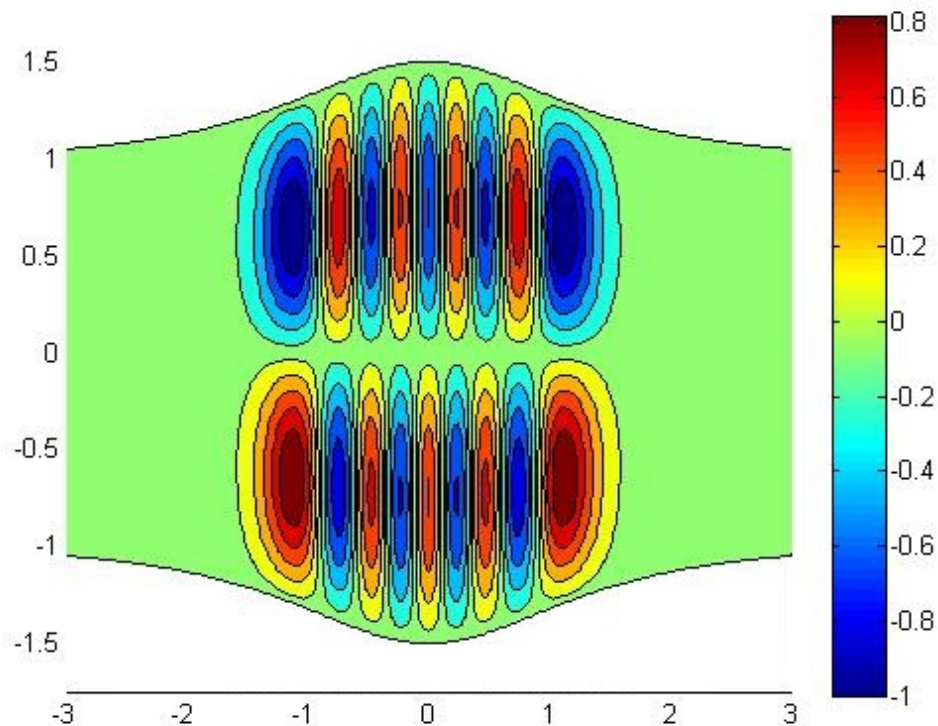


Figure 12: Contour plot of symmetric trapped modes for $n=2$.

4.3 Plotting the final solutions with Neumann boundary conditions

We will now compare these trappings with the symmetric and antisymmetric solutions of the Neumann boundary condition. Figures (13) and (14) illustrate resonance occurring at the surface boundary of the bulge region of the duct, unlike the Dirichlet case, in which resonance occurred in the whole region of the bulging duct. A better look at this difference, is to analyse the surface plots as illustrated in figures (15) and (16). From these graphs we can see the Neumann boundary conditions, suggest two resonating waves on each side of the boundary. We denoted in earlier chapters h_{\pm} to be the upper and lower boundaries of the duct (see figure (1)). If we analyse the symmetric graph first, we can see from figure (14) two resonating waves on each boundary $\pm h_{\pm}$. As a result figure (16) illustrates the waves decaying at $x \rightarrow \pm\infty$, similar to the Dirichlet case, but the thick dark areas represent the two waves from the side, in comparison to the Dirichlet the thin dark region illustrates the one wave decaying.

We will now consider trapped modes existing in the Neumann condition, for $n = 2$. This

Neumann bulge anti-symmetric n=1.jpg

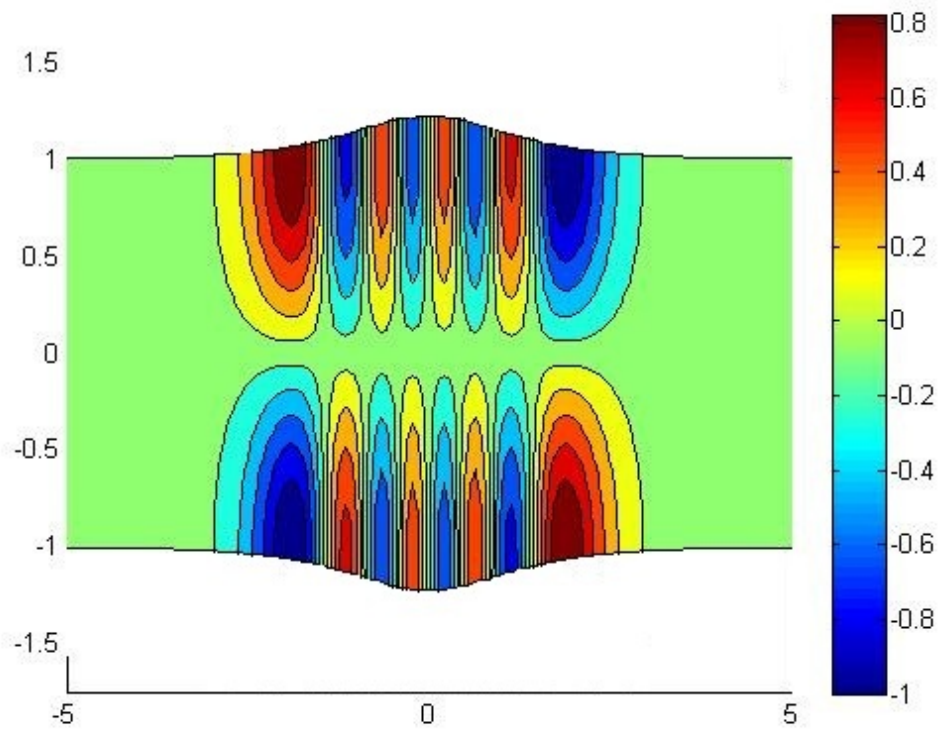


Figure 13: Contour plot of antisymmetric trapped modes, with Neumann boundary condition.

Neumann bulge symmetric n=1.jpg

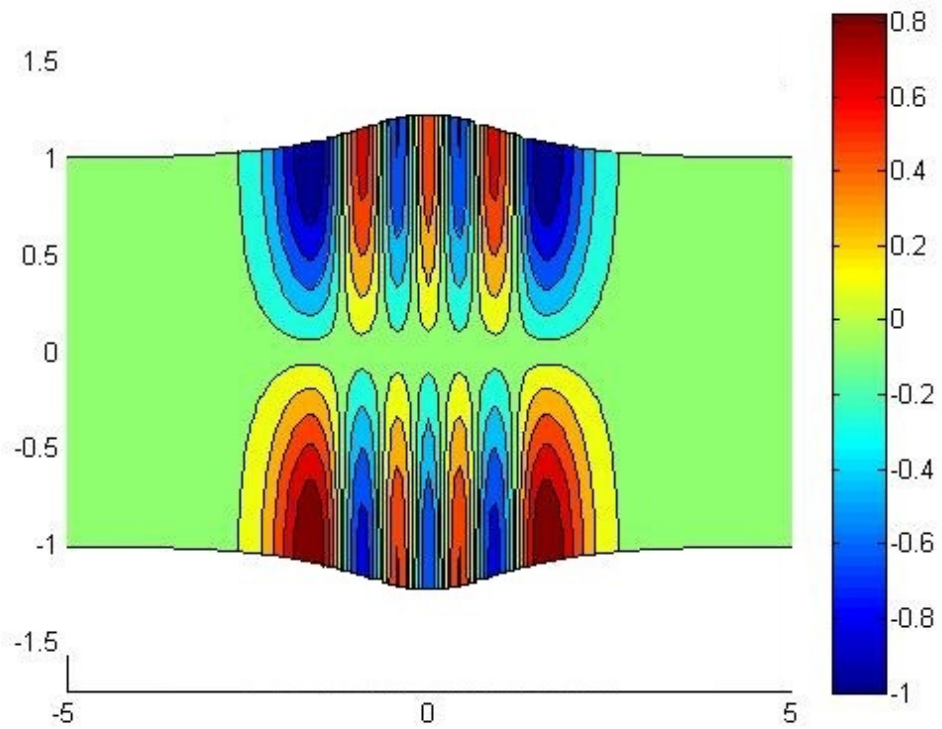


Figure 14: Contour plot of the symmetric trapped modes, with Neumann boundary condition for $n = 1$.

antisymmetric Neumann.jpg

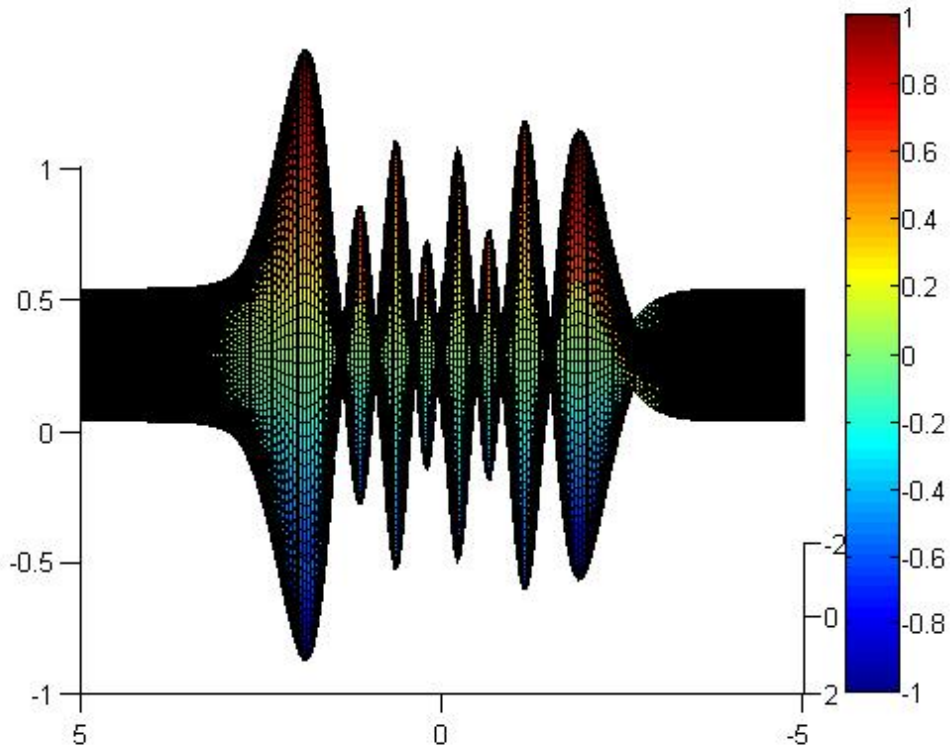


Figure 15: Surface plot of antisymmetric trapped modes, with Neumann boundary condition for $n = 1$, where we let $h_1 = 1.224$ and wavenumber $k = 1.500052$

symmetric Neumann.jpg

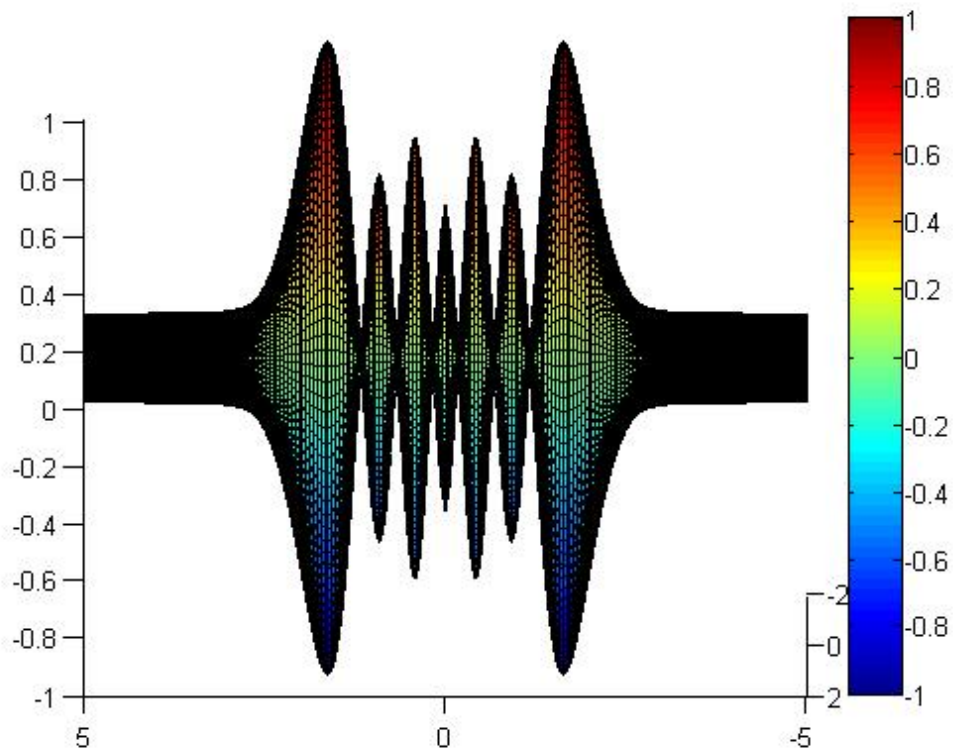


Figure 16: Surface plot of the symmetric trapped modes, with Neumann boundary condition for $n=1$, where we let $h_1 = 1.224$ and wavenumber $k = 1.479089$

Neumann bulge anti-symmetric n=2.jpg

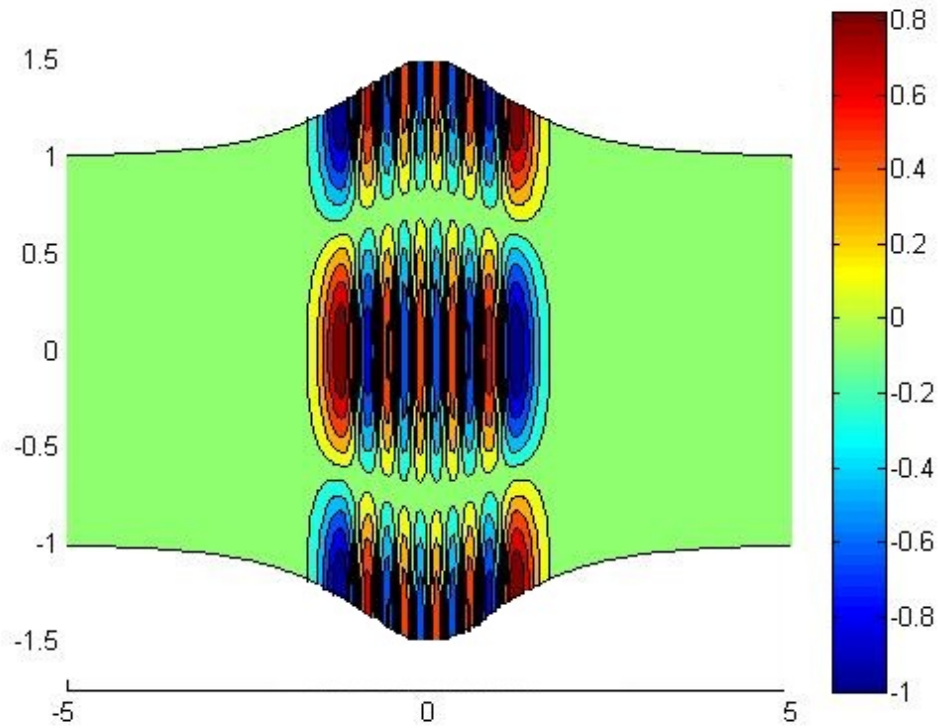


Figure 17: Contour plot of antisymmetric trapped modes, with Neumann boundary condition for $n=2$.

case again, is very similar to the Dirichlet case, with the main difference solutions now have three sets of propagating waves. Two occurring on the boundary, and one at the centre. We can deduce that as n increases, so does the number of trappings in the region, which again we would expect.

Neumann bulge symmetric n=2.jpg

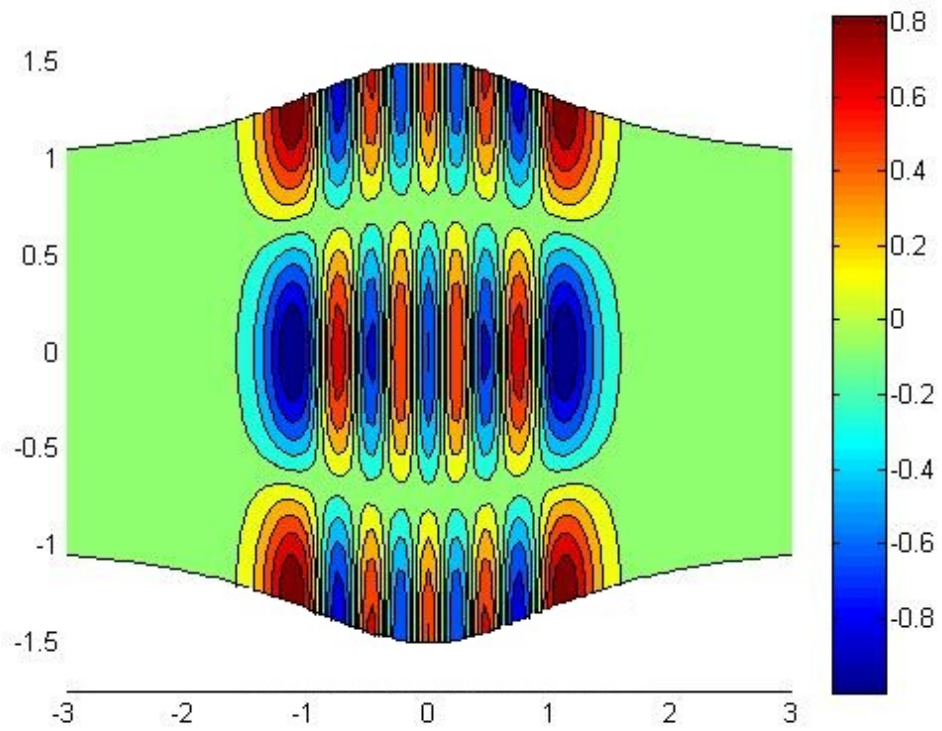


Figure 18: Contour plot of the symmetric trapped modes, with Neumann boundary condition for $n=2$.

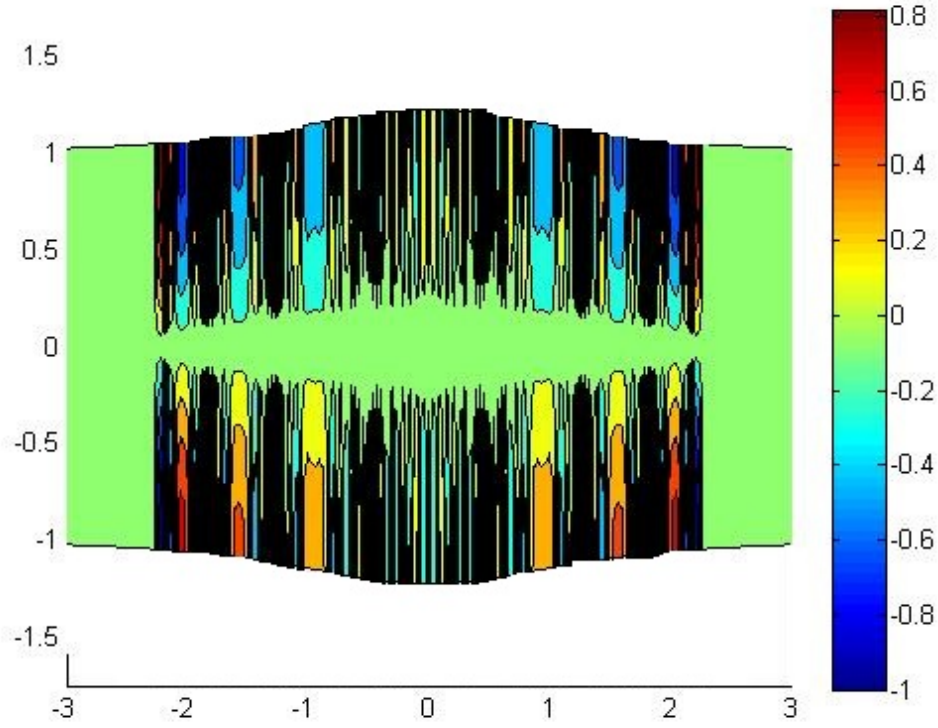


Figure 19: Contour plot of antisymmetric modes, with Neumann condition for $\epsilon = 0.001$.

4.4 Varying the small parameter ϵ

Research up until now, on this paper, has dealt with the small parameter $\epsilon = 0.1$, by varying this constant, such that it is even smaller, say 0.001, we find, a rich amount of trappings existing in the region of the bulge. Solutions of the wavenumbers will not be plotted for this paper, as solutions for each Z_n were plotted with marginal gaps between them. As a result, this suggested more trapped modes existed for waveguides, slowly varying as possible. This can be seen from figures (19) and (20) the strong detail in graphs show, many existing trappings occur within the region, and also the affects of the number of oscillations that occur. By letting $\epsilon \rightarrow 0$ we increase the number of oscillations within the region. This suggests resonance is greatest for slowly varying waveguides.

Physically this is plausible as it suggest the slower the variation in curvature of the waveguide is the more oscillations can exist.

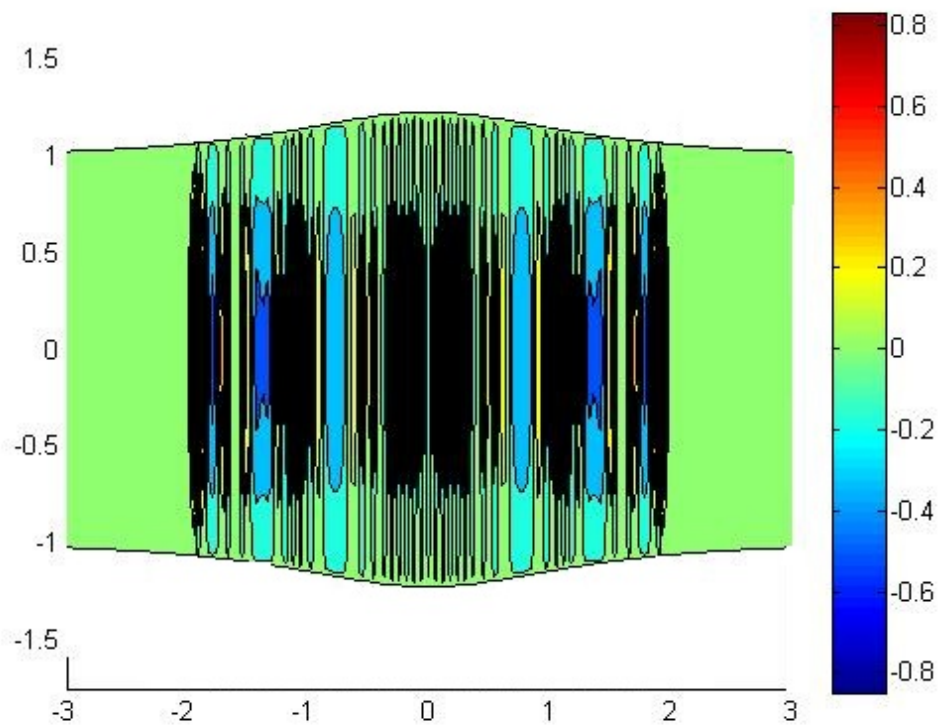


Figure 20: Contour plot of symmetric modes with Dirichlet condition for $\epsilon = 0.001$.

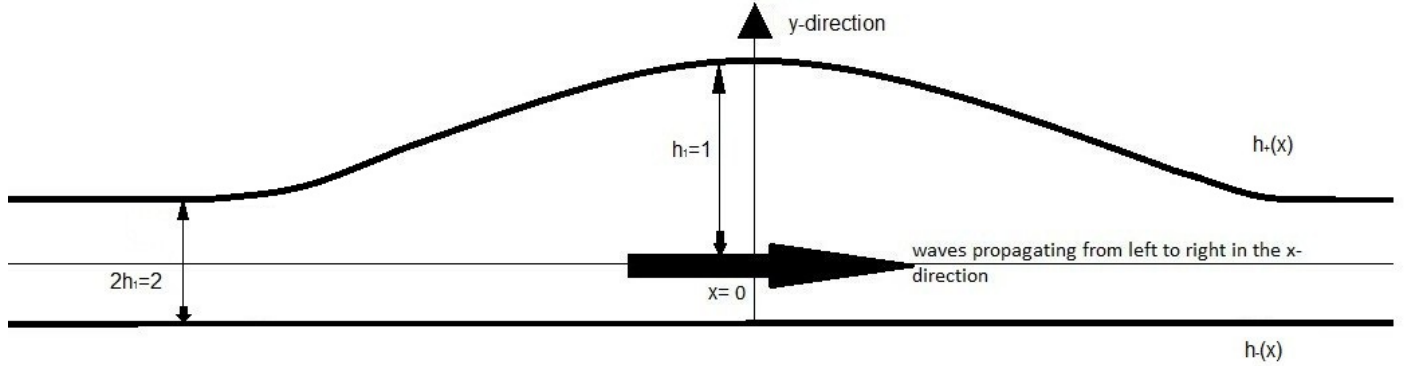


Figure 21: Waveguide with a bulging upper profile, and constant lower profile

4.5 Changing the geometrical structure

Having given detailed results on trappings for both Dirichlet and Neumann condition for a tapered duct, we can progress this theory, and explore existence of trappings for a different geometrical structure. One in particular, would be to consider the duct to be bulging in the upper profile, such that $\pm h_+ = 1 + (h_1 - 1)\text{sech}(x)$, but a constant in the lower profile, say $\pm h_- = 1$. As illustrated in figure (21).

By taking into account this new geometry, we change the program accordingly, noting that wavenumber k solutions remain the same. Plotting the symmetric and antisymmetric modes for the Dirichlet case, where $n = 1$, $\epsilon = 0.1$ and G_n remains the same, we find the solutions are very similar to that produced by a full bulging structure of the Dirichlet case. Figure (22) shows the antisymmetric case for the half bulging waveguide. The waves propagate at the centre of the waveguide, and eventually decay exponentially as the waves near the cut-off frequency. However it is clear to see the waves decay at a slower rate than in figure (10). Similarly for figure (23), resonating waves is found at the centre of the duct. A surface plot of the symmetric solution is found in figure (24), as we can see at $x \rightarrow \pm\infty$ the solution is graphically represented as a thicker line then in previous graphs.

We will now consider the solution of this new waveguide, when $n = 2$. We would expect the solution to bare a resemblance to the bulge case, with two solutions occuring. Figure (25) and (26) confirms this for antisymmetric and symmetric modes respectively. One thing to mention, the two graphs do not portray the same interval of x , hence why figure (26) does not look as slowly varying as figure (25), yet they are. The existence of trapped modes hold in this case.

constant n=1 anti-symmetric.jpg

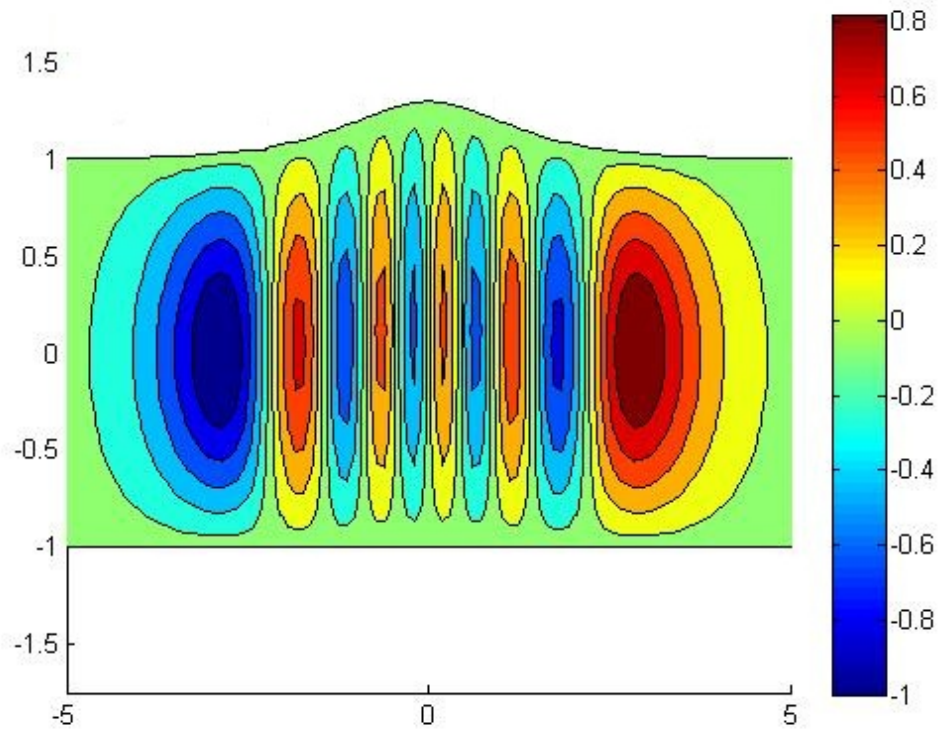


Figure 22: Contour plot of antisymmetric modes, with Dirichlet condition for the new geometrical structure.

constant n=1 symmetric.jpg

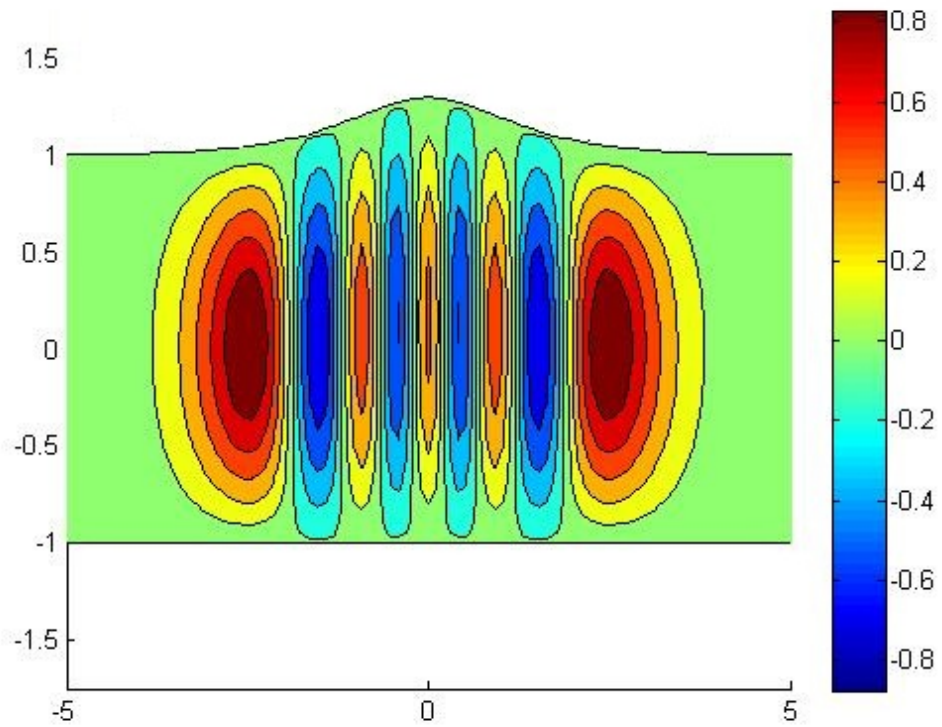


Figure 23: Contour plot of symmetric modes with Dirichlet condition for the new geometrical structure.

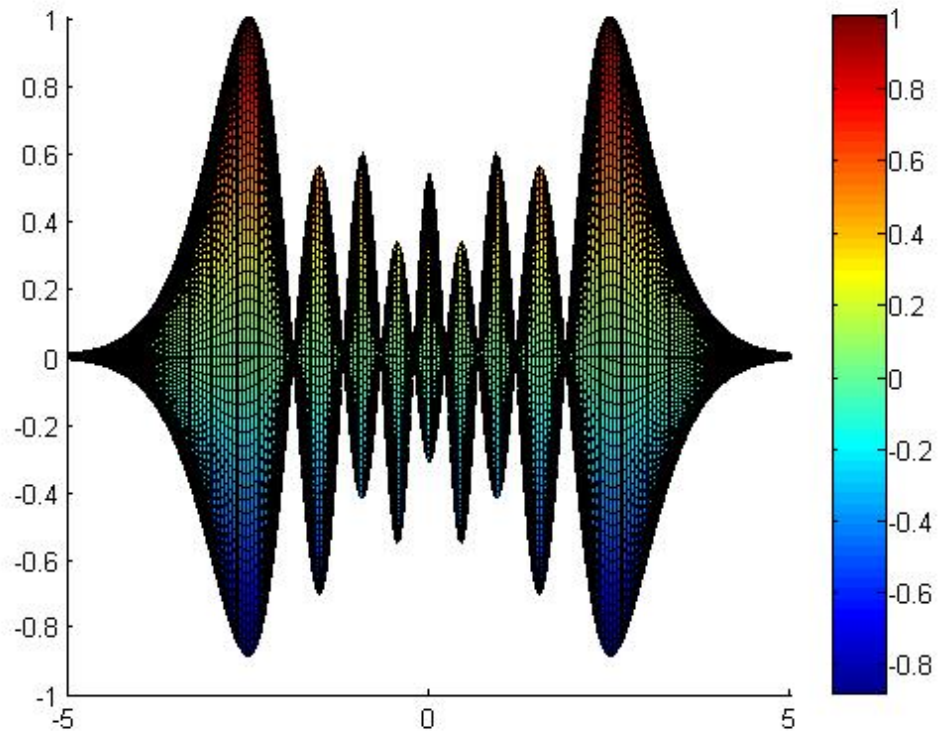


Figure 24: Surface plot of symmetric modes with Dirichlet condition for the new geometrical structure, where $h = 1.3012$ and $k = 1.54682$

constant n=2 anti-symmetric.jpg

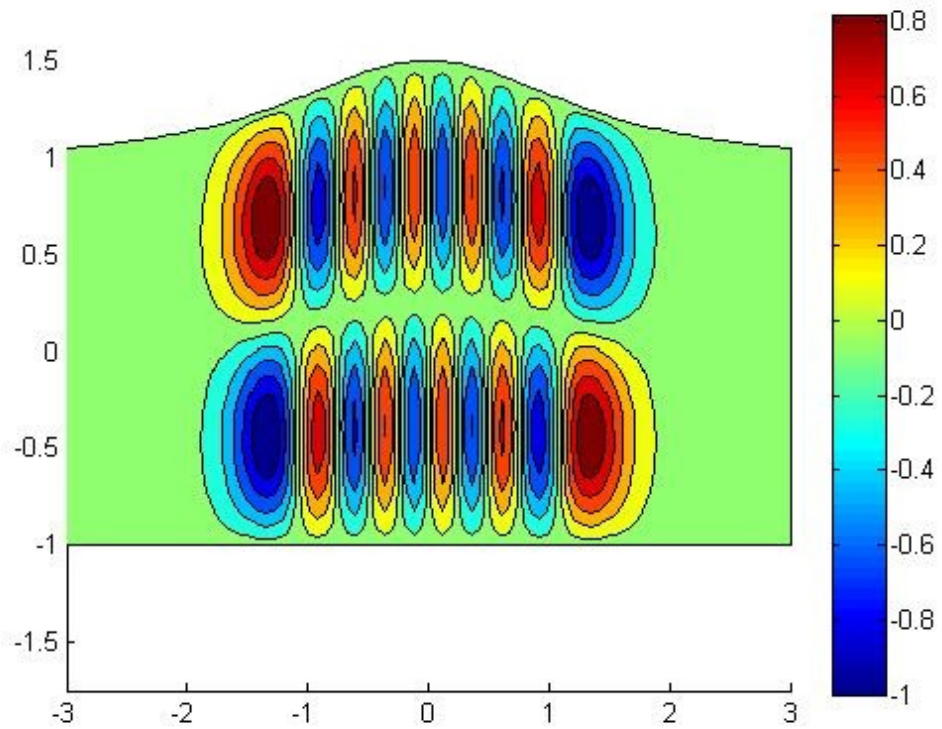


Figure 25: Contour plot of antisymmetric modes, with Dirichlet condition for the new geometrical structure, when $n = 2$.

constant n=2 symmetric.jpg

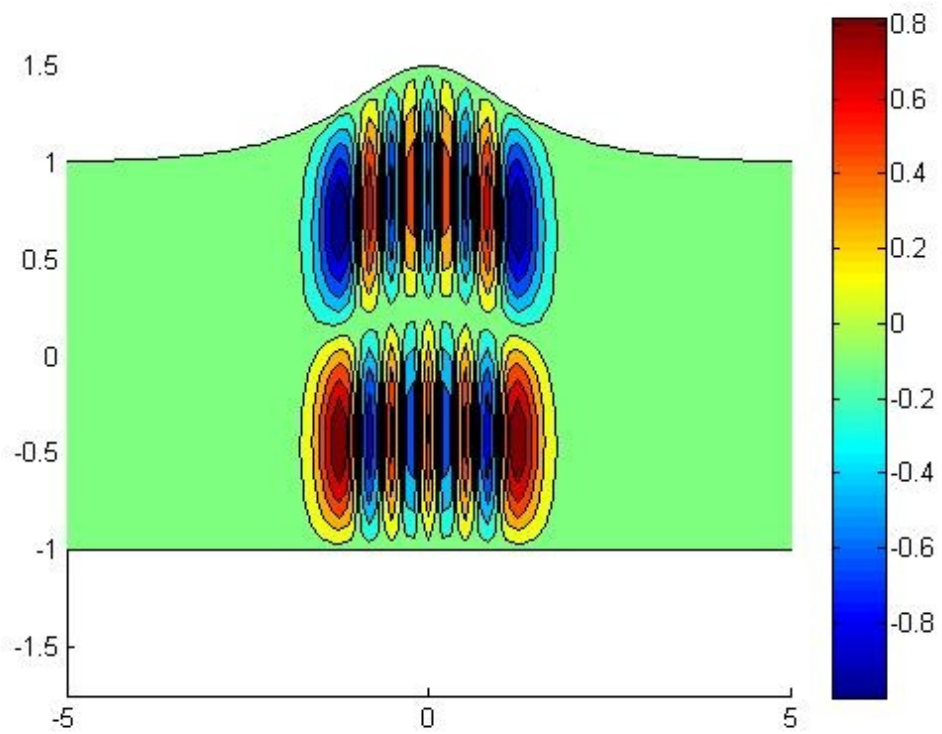


Figure 26: Contour plot of symmetric modes with Dirichlet condition for the new geometrical structure, when $n = 2$.

Neumann constant anti-symmetric n=1.jpg

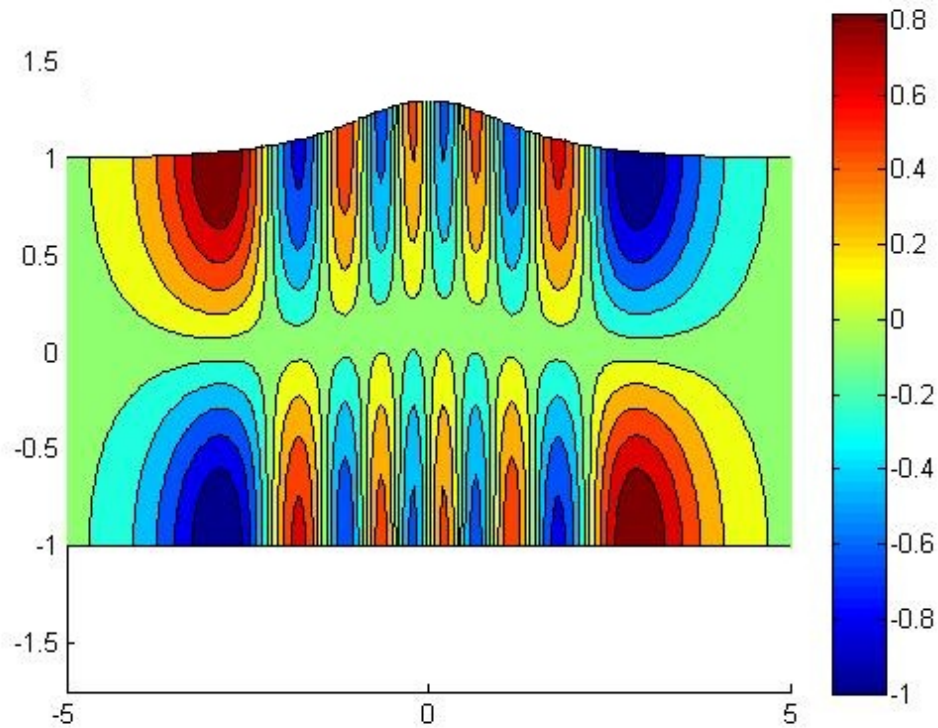


Figure 27: Contour plot of antisymmetric modes with Neumann condition for the new geometrical structure, when $n = 1$.

4.6 The Neumann boundary condition for the waveguide where $h_- = 1$

Having considered the possibilities of the Dirichlet condition, we may finally investigate trappings of the waveguide with a constant lower boundary for the Neumann condition. Figures (27) and (28) illustrate the solutions, which are found to be very similar to that found with the fully bulging waveguide. The trappings are found at the boundary of the waveguide, however one particular difference, is the exponential decay at the cut-off frequency. The propagating waves near the cut-off frequency, decay at a marginally slower rate for waveguides with a constant lower boundary then for waveguides with a bulge.

Neumann constant symmetric n=1.jpg

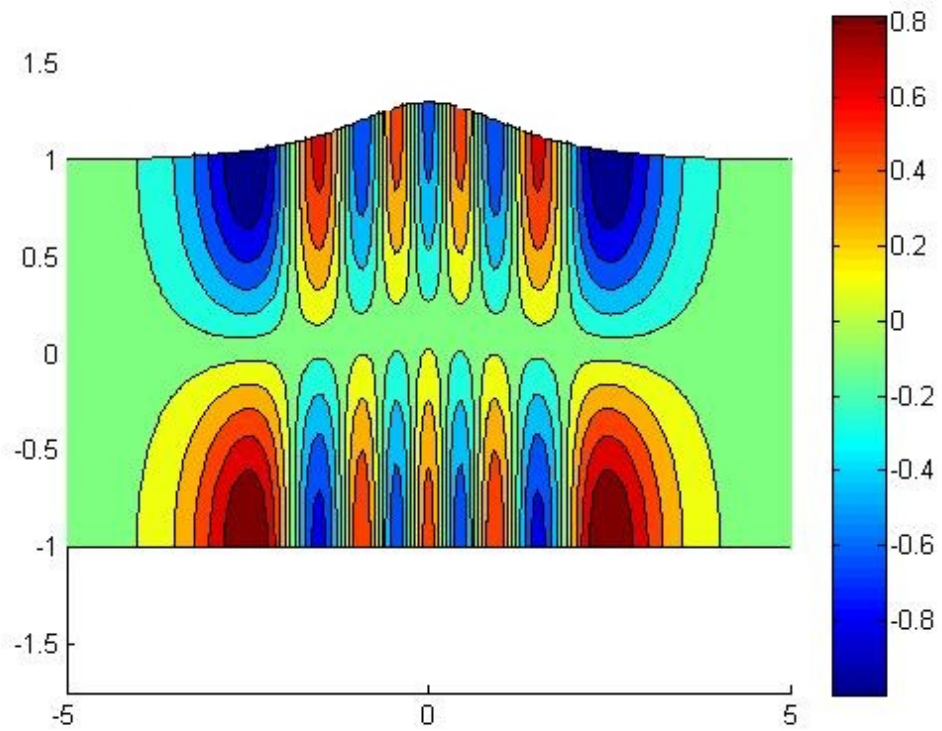


Figure 28: Contour plot of symmetric modes with Neumann condition for the new geometrical structure, when $n = 1$.

5 Conclusion

In this paper, we have shown trapped modes exist, for slowly varying waveguides of two different boundary conditions. Using an asymptotic expansion, we were able to solve the problem for various cases and identify the impact certain physical characteristics have on the solution. In particular, taking ϵ to be close to zero, leads to an increase in the number of oscillations leading to greater resonance. By considering two different shaped waveguides, we were able to compare the modes, and found similarities between the two cases. Further research in this paper can be made to investing trapping of energy for various geometrical structures. As though much work has already been made in this area [5, 3]. This paper also dealt with Dirichlet and Neumann boundary conditions, which help understand how they effect trapped modes. By investigating other boundary conditions, such as the mixed problem, we can understand the occurrence of trappings in more detail, and apply this work to applications in resonance in acoustic waveguides.

Unfortunately, we were unable to carry out further numerical work. Having now found the solution to the problem through a perturbation method, we could verify the accuracy through another more advance numerical technique, the spectral method. We will not go into details over the aspects involved, however in Craster's paper [2], the use of Chebyshev-Laguerre spectral method would verify the calculations made in this paper were correct.

Studying trapped modes in waveguides, is a field, with many applications, much research has gone into the possibilities for futher work. Some areas in particular, would involve investigating anti-symmetric waveguides. As mentioned earlier this paper dealt with the symmtric waveguide throughout, as this helped understand the existence of trapped modes, however finding modes for antisymmetric waveguides, is an area of great interest, as its applications would be useful and realistic in not only acoustic waveguides, but other areas, such as electromagnetic, quantum and water waves.

6 First Appendix

List of Airy solutions and the first derivative solutions			
Z_1	-2.338107410459764	Z'_1	-1.018792971647472
Z_2	-4.087949444130973	Z'_2	-3.248197582179841
Z_3	-5.520559828095556	Z'_3	-4.820099211178738
Z_4	-6.786708090071763	Z'_4	-6.163307355639495
Z_5	-7.944133587120851	Z'_5	-7.372177255047778
Z_6	-9.022650853340979	Z'_6	-8.488486734019723
Z_7	-10.040174341558082	Z'_7	-9.535449052433547
Z_8	-11.008524303733266	Z'_8	-10.527660396957408
Z_9	-11.936015563236262	Z'_9	-11.475056633480246
Z_{10}	-12.828776752865757	Z'_{10}	-12.384788371845749
Z_{11}	-13.691489035210719	Z'_{11}	-13.262218961665209
Z_{12}	-14.527829951775335	Z'_{12}	-14.111501970462996
Z_{13}	-15.340755135977997	Z'_{13}	-14.935937196720518
Z_{14}	-16.132685156945772	Z'_{14}	-15.738201373692538
Z_{15}	-16.905633997429945	Z'_{15}	-16.520503825433796
Z_{16}	-17.661300105697059	Z'_{16}	-17.284695050216438
Z_{17}	-18.401132599207116	Z'_{17}	-18.032344622504393
Z_{18}	-19.126380474246954	Z'_{18}	-18.764798437665952
Z_{19}	-19.838129891721501	Z'_{19}	-19.483221656567235
Z_{20}	-20.537332907677566	Z'_{20}	-20.188631509463374
Z_{21}	-21.224829943642099	Z'_{21}	-20.881922755516740
Z_{22}	-21.901367595585132	Z'_{22}	-21.563887723198977
Z_{23}	-22.567612917496504	Z'_{23}	-22.235232285348914
Z_{24}	-23.224165001121680	Z'_{24}	-22.896588738874620

7 Bibliography

This paper is largely based on the works made by Dr. Nick Biggs using the paper of the same name.

References

- [1] N.Biggs, "Wave reflection and trapping in a two-dimensional duct,"
- [2] J.Postnova, R.V Craster, "Trapped modes in topographically varying elastic waveguides," *Wave Motion* 44 (2007) 205-221
- [3] J.Postnova, R.V Craster, "Trapped modes in elastic plates, oceans and quantum waveguides," *Wave Motion* 45 (2008) 565-579
- [4] A.T.I. Adamou, D. Gridin, R.V Craster, "Acoustic quasi-modes in slowly varying cylindrical tubes," *Q.JI Mech.appl.math*, Vol.58 No.3 (2005)
- [5] Y. Dan, W. Koch, C.S M. Linton & M. McIver, "Complex resonances and trapped modes in ducted domains,"
- [6] S.Hein & W. Koch, "Acoustic resonances and trapped modes in pipes and tunnels," *J. Fluid Mech.* (2008), vol. 605, pp. 401-428.
- [7] Kopka, H., Daly P.W., *Perturbation Methods*, E.J.Hinch, Cambridge text in applied mathematics, Mexico, 1991, pp 127-140.